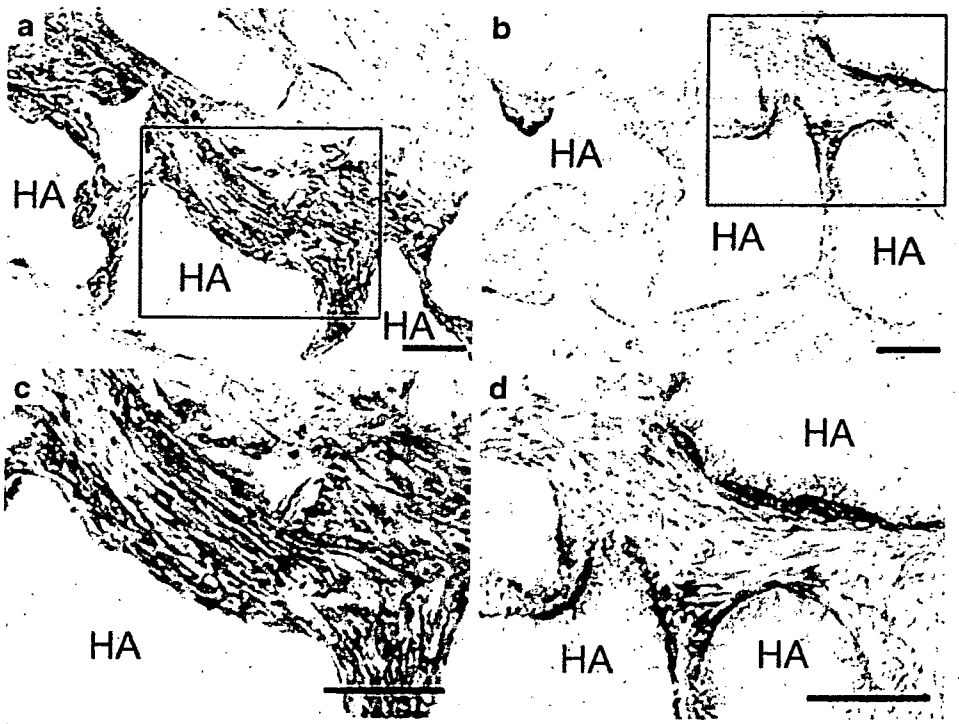

Fig. 8 Sections prepared from tissues in which HPDL2 (**a**, **c**) or M-HPL1 (**b**, **d**) were transplanted with hydroxyapatite particles (*HA*) into SCID mice for 4 weeks. Immunostaining with anti-human vimentin monoclonal antibody. The *boxed areas* in **a**, **b** are shown at higher magnification in **c**, **d**, respectively. Note that HPDL2 aligned in an organized manner, but M-HPL1 showed disorganized alignment. *Bars* 100 μm

has been identified as the responsible gene in MFS2 (Mizuguchi et al. 2004). The present patient has a heterozygous mutation in *FBN1* (Fig. 1f); this mutation results in a missense substitution (N2144S; Fig. 1g), clearly identifying the disease as MFS1.

Since *FBN1* is a large gene with 65 exons, direct sequencing of all the exons to identify mutations is time-consuming and costly. Therefore, we have performed DHPLC to screen for mutations in *FBN1*. In total, 65 amplicons for *FBN1* and 8 amplicons for *TGFBR2* have been synthesized by using specific primers by PCR. Heteroduplex formation has been identified in the product of exon 52 in *FBN1* by DHPLC (Fig. 1e). By using this method, systems have previously been developed to screen 20 congenital disorders (Kosaki et al. 2005). The present DHPLC method is a sensitive and powerful tool that allows the screening of gene mutations before direct sequencing; this is especially useful for large genes such as *FBN1*.

Cells isolated from the PDL of our MFS1 patient and of healthy volunteers have both shown increased ALP activity and mineralization in the cell differentiation medium. PDL cells are known to show an osteoblastic phenotype when cultured under these conditions (Cho et al. 1992; Giannopoulou and Cimasoni 1996; Nohutcu et al. 1997; Chien et al. 1999). After immortalization of cells by introducing *hTERT* and *Bmi-1*, both HPDL2 and M-HPL1 express PDL-related genes, viz., *POSTN* (Fujii et al. 2006), *ASPN* (Yamada et al. 2001), *COL12A1* (Fujii et al. 2006), *BGLAP* (Fujii et al. 2006), *BSP* (Yokoi et al. 2007), and *COL1A1* (Yokoi et al. 2007; Fig. 4a). These observations demonstrate that both types of cells have the characteristic phenotype of cultured PDL cells. However, *POSTN*, *COL12A1*, *BGLAP*, and *COL1A1*

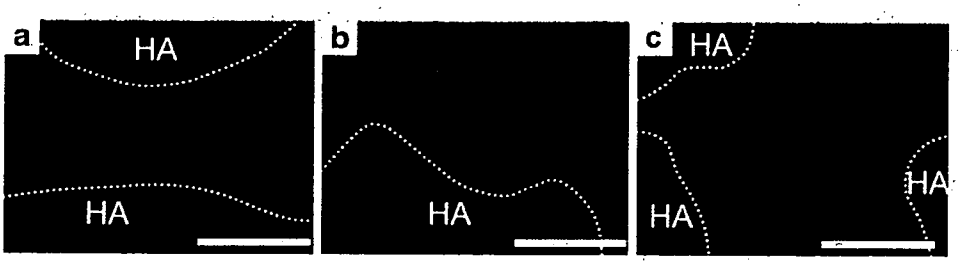

Fig. 9 Sections prepared from tissues in which HPDL2 (**a**) or M-HPL1 (**b**) were transplanted with hydroxyapatite particles (*HA*) into SCID mice for 4 weeks (*dotted lines* outline of HA). Immunostaining with anti-human fibrillin-1 antibody. Note the irregular microfibril assembly in the tissue implanted with M-HPL1 (**b**) but not in that with HPDL2 (**a**). **c** Sections prepared from tissues in which HA particles without cells were transplanted into SCID mice for 4 weeks. Note the absence of immunostaining with anti-human fibrillin-1 antibody (*dotted lines* outline of HA). *Bars* 50 μm

exhibit a lower expression in M-HPL1 than in HPDL2, and *OPN* is hardly expressed in M-HPL1 (Fig. 4a). We now need to examine whether PDL cells isolated from other MFS1 patients reveal a similar down-regulation of these genes.

Recently, attempts have been made to establish immortalized PDL cells by introducing *hTERT* (Berry et al. 2003; Kamata et al. 2004; Fujita et al. 2005; Saito et al. 2005; Fujii et al. 2006; Zhang et al. 2006). Cyclin-dependent kinase inhibitors $p16^{Ink4a}$ and $p21^{WAF1}$ induce premature senescence in human cells by telomere-independent mechanisms (Ramirez et al. 2001). As Bmi-1 can down-regulate the expression of $p16^{Ink4a}$ and $p14^{ARF}$ (Jacobs et al. 1999), it has been used to extend the life span of bovine and human cells (Dimri et al. 2002; Cudre-Mauroux et al. 2003; Itahana et al. 2003; Saito et al. 2005; Haga et al. 2007). Thus, in this study, we have immortalized human PDL cells with retrovirus-mediated transduction of both *hTERT* and *Bmi-1*. By using this method, both HPDL2 and M-HPL1 have been immortalized while maintaining their original gene expressions (Fig. 2c, Fig. 4a), as reported in cementoblast progenitor cells (Saito et al. 2005).

In MFS1, the activation of TGF-β signaling has been suggested as the pathogenesis for mitral valve prolapse and emphysema (Neptune et al. 2003; Ng et al. 2004). Mutations in *FBN1* alter or preclude matrix alteration of the latent complex of TGF-β, rendering TGF-β more accessible for activation (Neptune et al. 2003). In this study, activated TGF-β has been shown to be more abundant in M-HPL1 than in HPDL2 (Fig. 6e, f), suggesting that activated TGF-β signaling occurs in the PDL of our MFS1 patient.

N2144S in fibrillin-1 is predicted to alter one of the key calcium-binding residue ligands within the 32th cbEGF domain (Kettle et al. 1999; Yuan et al. 2002). This mutation is known to increase flexibility in the peptide backbone (Yuan et al. 2002). Attempts should be made to link this mutation and the disorganized cell alignment and microfibril assembly seen in this study.

OPN expression is lower in M-HPL1 than in HPDL2 (Fig. 4a). The exact reason for this difference is not known. However, TGF-β blockade has been reported significantly to enhance the BMP-2-induced upregulation of *OPN* expression, suggesting that TGF-β is a negative regulator on *OPN* expression (Shen et al. 2007). An examination is required of whether decreased expression of *OPN* (Fig. 4a) is mediated by the enhanced TGF-β activation in M-HPL1 (Fig. 6). Moreover, since no study has reported a relationship between fibrillin-1 and *OPN* expression, an investigation of *OPN* expression in M-HPL1 would be of interest after transfecting wild-type fibrillin-1 or during the culture of these cells on the fibrillin-1-coated dishes.

In summary, PDL cells have been isolated from an MFS1 patient with a heterozygous mutation in the 32th cbEGF domain (N2144S). These PDL cells have been immortalized by transducing human *mi-1* and *hTERT*. The present immortalized PDL cells show increased levels of activated TGF-β and should provide a powerful tool for the clarification of the biological roles of the elastic system fibers in PDLs and the pathogenesis of periodontitis in MFS1.

Acknowledgements The authors thank Dr. K. Ohyama (former Professor of Tokyo Medical and Dental University), Dr. S. Yamada (Osaka University), and Professor S. Murakami (Osaka University) for their valuable advice and discussion. The authors are also grateful to Professor T. Yoda (Saitama Medical University) and Dr. Y. Fukushima (Saitama Medical University) for organizing the tooth samples and providing the medical history of the patient. The authors also express their gratitude to Marfan Network Japan (MNJ) for their cooperation in the present research. Additional thanks are extended to Dr. T. Yokoi (Aichi Gakuin University), Dr. T. Tsubakimoto (Kanagawa Dental College), Dr. E. Nishida (Aichi Gakuin University), Dr. K. Kosaka (Kanagawa Dental College), and Dr. M. Aino (Aichi Gakuin University) for their technical assistance.

References

Bauss O, Sadat-Khonsari R, Fenske C, Engelke W, Schwestka-Polly R (2004) Temporomandibular joint dysfunction in Marfan syndrome. Oral Surg Oral Med Oral Pathol Oral Radiol Endod 97:592–598

Beertsen W, McCulloch CA, Sodek J (1997) The periodontal ligament: a unique, multifunctional connective tissue. Periodontol 2000:20–40

Berry JE, Zhao M, Jin Q, Foster BL, Viswanathan H, Somerman MJ (2003) Exploring the origins of cementoblasts and their trigger factors. Connect Tissue Res 44 (Suppl 1):97–102

Boileau C, Jondeau G, Babron MC, Coulon M, Alexandre JA, Sakai L, Melki J, Delorme G, Dubourg O, Bonaiti-Pellie C, Bourdarias JP, Junienet C (1993) Autosomal dominant Marfan-like connective-tissue disorder with aortic dilation and skeletal anomalies not linked to the fibrillin genes. Am J Hum Genet 53:46–54

Chien HH, Lin WL, Cho MI (1999) Interleukin-1beta-induced release of matrix proteins into culture media causes inhibition of mineralization of nodules formed by periodontal ligament cells in vitro. Calcif Tissue Int 64:402–413

Cho MI, Matsuda N, Lin WL, Moshier A, Ramakrishnan PR (1992) In vitro formation of mineralized nodules by periodontal ligament cells from the rat. Calcif Tissue Int 50:459–467

Cudre-Mauroux C, Occhiodoro T, Konig S, Salmon P, Bernheim L, Trono D (2003) Lentivector-mediated transfer of Bmi-1 and telomerase in muscle satellite cells yields a Duchenne myoblast cell line with long-term genotypic and phenotypic stability. Hum Gene Ther 14:1525–1533

Dietz HC, Cutting GR, Pyeritz RE, Maslen CL, Sakai LY, Corson GM, Puffenberger EG, Hamosh A, Nanthakumar EJ, Curristin SM, Stetten G, Meyers DA, Francomano CA (1991) Marfan syndrome caused by a recurrent de novo missense mutation in the fibrillin gene. Nature 352:337–339

Dimri GP, Martinez JL, Jacobs JJ, Keblusek P, Itahana K, Van Lohuizen M, Campisi J, Wazer DE, Band V (2002) The Bmi-1 oncogene induces telomerase activity and immortalizes human mammary epithelial cells. Cancer Res 62:4736–4745

Flanders KC, Thompson NL, Cissel DS, Van Obberghen-Schilling E, Baker CC, Kass ME, Ellingsworth LR, Roberts AB, Sporn MB (1989) Transforming growth factor-beta 1: histochemical local-

ization with antibodies to different epitopes. J Cell Biol 108: 653–660
Freeman E (1998) Periodontium. In: Ten Cate AR (ed) Oral histology: development, structure, and function, 5th edn. Mosby, St. Louis, pp 253–286
Fujii S, Maeda H, Wada N, Kano Y, Akamine A (2006) Establishing and characterizing human periodontal ligament fibroblasts immortalized by SV40T-antigen and hTERT gene transfer. Cell Tissue Res 324:117–125
Fujita T, Otsuka-Tanaka Y, Tahara H, Ide T, Abiko Y, Mega J (2005) Establishment of immortalized clonal cells derived from periodontal ligament cells by induction of the hTERT gene. J Oral Sci 47:177–184
Fullmer HM, Sheetz JH, Narkates AJ (1974) Oxytalan connective tissue fibers: a review. J Oral Pathol 3:291–316
Giannopoulou C, Cimasoni G (1996) Functional characteristics of gingival and periodontal ligament fibroblasts. J Dent Res 75: 895–902
Haga K, Ohno S, Yugawa T, Narisawa-Saito M, Fujita M, Sakamoto M, Galloway DA, Kiyono T (2007) Efficient immortalization of primary human cells by p16-specific short hairpin RNA or Bmi-1, combined with introduction of hTERT. Cancer Sci 98: 147–154
Handa K, Saito M, Yamauchi M, Kiyono T, Sato S, Teranaka T, Sampath Narayanan A (2002) Cementum matrix formation in vivo by cultured dental follicle cells. Bone 31:606–611
Hewett DR, Lynch JR, Smith R, Sykes BC (1993) A novel fibrillin mutation in the Marfan syndrome which could disrupt calcium binding of the epidermal growth factor-like module. Hum Mol Genet 2:475–477
Itahana K, Zou Y, Itahana Y, Martinez JL, Beausejour C, Jacobs JJ, Van Lohuizen M, Band V, Campisi J, Dimri GP (2003) Control of the replicative life span of human fibroblasts by p16 and the polycomb protein Bmi-1. Mol Cell Biol 23:389–401
Jacobs JJ, Kieboom K, Marino S, DePinho RA, Lohuizen M van (1999) The oncogene and Polycomb-group gene bmi-1 regulates cell proliferation and senescence through the ink4a locus. Nature 397:164–168
Kamata N, Fujimoto R, Tomonari M, Taki M, Nagayama M, Yasumoto S (2004) Immortalization of human dental papilla, dental pulp, periodontal ligament cells and gingival fibroblasts by telomerase reverse transcriptase. J Oral Pathol Med 33:417–423
Kapila YL, Kapila S, Johnson PW (1996) Fibronectin and fibronectin fragments modulate the expression of proteinases and proteinase inhibitors in human periodontal ligament cells. Matrix Biol 15:251–261
Kawamoto T, Shimizu M (2000) A method for preparing 2- to 50-micron-thick fresh-frozen sections of large samples and undecalcified hard tissues. Histochem Cell Biol 113:331–339
Kettle S, Yuan X, Grundy G, Knott V, Downing AK, Handford PA (1999) Defective calcium binding to fibrillin-1: consequence of an N2144S change for fibrillin-1 structure and function. J Mol Biol 285:1277–1287
Kielty CM, Sherratt MJ, Shuttleworth CA (2002) Elastic fibres. J Cell Sci 115:2817–2828
Kosaki K, Udaka T, Okuyama T (2005) DHPLC in clinical molecular diagnostic services. Mol Genet Metab 86:117–123
Kyo S, Nakamura M, Kiyono T, Maida Y, Kanaya T, Tanaka M, Yatabe N, Inoue M (2003) Successful immortalization of endometrial glandular cells with normal structural and functional characteristics. Am J Pathol 163:2259–2269
Maslen CL, Corson GM, Maddox BK, Glanville RW, Sakai LY (1991) Partial sequence of a candidate gene for the Marfan syndrome. Nature 352:334–337
Mecham RP (1991) Elastin synthesis and fiber assembly. Ann N Y Acad Sci 624:137–146
Miyazono K, Ichijo H, Heldin CH (1993) Transforming growth factor-beta: latent forms, binding proteins and receptors. Growth Factors 8:11–22
Mizuguchi T, Collod-Beroud G, Akiyama T, Abifadel M, Harada N, Morisaki T, Allard D, Varret M, Claustres M, Morisaki H, Ihara M, Kinoshita A, Yoshiura K, Junien C, Kajii T, Jondeau G, Ohta T, Kishino T, Furukawa Y, Nakamura Y, Niikawa N, Boileau C, Matsumoto N (2004) Heterozygous TGFBR2 mutations in Marfan syndrome. Nat Genet 36:855–860
Neptune ER, Frischmeyer PA, Arking DE, Myers L, Bunton TE, Gayraud B, Ramirez F, Sakai LY, Dietz HC (2003) Dysregulation of TGF-beta activation contributes to pathogenesis in Marfan syndrome. Nat Genet 33:407–411
Ng CM, Cheng A, Myers LA, Martinez-Murillo F, Jie C, Bedja D, Gabrielson KL, Hausladen JM, Mecham RP, Judge DP, Dietz HC (2004) TGF-beta-dependent pathogenesis of mitral valve prolapse in a mouse model of Marfan syndrome. J Clin Invest 114: 1586–1592
Nohutcu RM, McCauley LK, Koh AJ, Somerman MJ (1997) Expression of extracellular matrix proteins in human periodontal ligament cells during mineralization in vitro. J Periodontol 68:320–327
Nollen GJ, Mulder BJ (2004) What is new in the Marfan syndrome? Int J Cardiol 97 (Suppl 1):103–108
Pyeritz RE (2000) The Marfan syndrome. Annu Rev Med 51:481–510
Ramirez RD, Morales CP, Herbert BS, Rohde JM, Passons C, Shay JW, Wright WE (2001) Putative telomere-independent mechanisms of replicative aging reflect inadequate growth conditions. Genes Dev 15:398–403
Saito Y, Yoshizawa T, Takizawa F, Ikegame M, Ishibashi O, Okuda K, Hara K, Ishibashi K, Obinata M, Kawashima H (2002) A cell line with characteristics of the periodontal ligament fibroblasts is negatively regulated for mineralization and Runx2/Cbfa1/Osf2 activity, part of which can be overcome by bone morphogenetic protein-2. J Cell Sci 115:4191–4200
Saito M, Handa K, Kiyono T, Hattori S, Yokoi T, Tsubakimoto T, Harada H, Noguchi T, Toyoda M, Sato S, Teranaka T (2005) Immortalization of cementoblast progenitor cells with Bmi-1 and TERT. J Bone Miner Res 20:50–57
Sawada T, Sugawara Y, Asai T, Aida N, Yanagisawa T, Ohta K, Inoue S (2006) Immunohistochemical characterization of elastic system fibers in rat molar periodontal ligament. J Histochem Cytochem 54:1095–1103
Shen ZJ, Kim SK, Jun DY, Park W, Kim YH, Malter JS, Moon BJ (2007) Antisense targeting of TGF-beta1 augments BMP-induced upregulation of osteopontin, type I collagen and Cbfa1 in human Saos-2 cells. Exp Cell Res 313:1415–1425
Sherr CJ, DePinho RA (2000) Cellular senescence: mitotic clock or culture shock? Cell 102:407–410
Shiga M, Kapila YL, Zhang Q, Hayami T, Kapila S (2003) Ascorbic acid induces collagenase-1 in human periodontal ligament cells but not in MC3T3-E1 osteoblast-like cells: potential association between collagenase expression and changes in alkaline phosphatase phenotype. J Bone Miner Res 18:67–77
Staszyk C, Gasse H (2004) Oxytalan fibres in the periodontal ligament of equine molar cheek teeth. Anat Histol Embryol 33:17–22
Straub AM, Grahame R, Scully C, Tonetti MS (2002) Severe periodontitis in Marfan's syndrome: a case report. J Periodontol 73: 823–826
Ten Cate AR (1998) Hard tissue formation and destruction. In: Ten Cate AR (ed) Oral histology: development, structure, and function, 5th edn. Mosby, St. Louis, pp 69–77
Udaka T, Samejima H, Kosaki R, Kurosawa K, Okamoto N, Mizuno S, Makita Y, Numabe H, Toral JF, Takahashi T, Kosaki K (2005) Comprehensive screening of CREB-binding protein gene mutations among patients with Rubinstein-Taybi syndrome using

denaturing high-performance liquid chromatography. Congenit Anom 45:125–131

Westling L, Mohlin B, Bresin A (1998) Craniofacial manifestations in the Marfan syndrome: palatal dimensions and a comparative cephalometric analysis. J Craniofac Genet Dev Biol 18:211–218

Yamada S, Murakami S, Matoba R, Ozawa Y, Yokokoji T, Nakahira Y, Ikezawa K, Takayama S, Matsubara K, Okada H (2001) Expression profile of active genes in human periodontal ligament and isolation of PLAP-1, a novel SLRP family gene. Gene 275:279–286

Yokoi T, Saito M, Kiyono T, Iseki S, Kosaka K, Nishida E, Tsubakimoto T, Harada H, Eto K, Noguchi T, Teranaka T (2007) Establishment of immortalized dental follicle cells for generating periodontal ligament in vivo. Cell Tissue Res 327:301–311

Yuan X, Werner JM, Lack J, Knott V, Handford PA, Campbell ID, Downing AK (2002) Effects of the N2144S mutation on backbone dynamics of a TB-cbEGF domain pair from human fibrillin-1. J Mol Biol 316:113–125

Zhang X, Soda Y, Takahashi K, Bai Y, Mitsuru A, Igura K, Satoh H, Yamaguchi S, Tani K, Tojo A, Takahashi TA (2006) Successful immortalization of mesenchymal progenitor cells derived from human placenta and the differentiation abilities of immortalized cells. Biochem Biophys Res Commun 351:853–859

and NF-κB, might be regulated by S nitrosylation. S nitrosylation inhibits the kinase activity of apoptosis signal regulation kinase 1 (ASK1) through inhibition of its binding to substrates (38). ASK1 is known as an important regulator of the TRAF6-p38 mitogen-activated protein kinase (MAPK) pathway downstream of TLR4 and is also involved in modulation of both the NF-κB and apoptotic pathways downstream of TLR2 (19, 34). Caspse-1 was recently found to be involved in TLR2- and TLR4-mediated signal transduction of the MyD88-dependent pathway through the cleavage of the TIR domain-containing adaptor protein TIRAP (also known as Mal) (37). Caspase-1 also undergoes S nitrosylation at a cysteine residue within the enzymatic active site, suppressing its proteolytic activity (6, 31). Thus, it is possible that NO provides regulatory effects on the multiple steps of TLR-mediated innate immune signaling through S nitrosylation. In this study, we therefore designed experiments to determine the effect of S nitrosylation on TLR signaling. We further investigated how S nitrosylation affects TLR-initiated immune responses in vivo. We report here that S nitrosylation controls TLR signaling through redox-sensitive and reversible suppression of the MyD88 pathway, which facilitates appropriate control of acute-phase inflammatory responses in vivo.

MATERIALS AND METHODS

Reagents and cell culture. N^G-Monomethyl-L-arginine monoacetate (L-NMMA), *S*-nitrosoglutathione (GSNO), glutathione (GSH), *N*-ethylmaleimide, coumermycin A, *N*-acetyl L-cysteine (NAC), ascorbic acid, and diphenyleneiodonium (DPI) were obtained from Sigma-Aldrich. SNAP (5-nitroso-*N*-acetyl-D,L-penicillamine) was purchased from Cayman Chemical. ODQ (1*H*-[1,2,4]oxadiazolo[4,3-*a*]quinoxalin-1-one) and KT5823 were obtained from Calbiochem. Preparation of TLR ligands, including highly purified *Escherichia coli* LPS, *Salmonella* LPS, Pam_3CSK_4, macrophage-activating lipopeptide 2 (MALP-2), and *Salmonella enterica* serovar Typhimurium flagellin, was as described previously (18). Recombinant human IL-1β was from R&D Systems. Human aortic endothelial cells (HAECs) and human embryonic kidney 293 (HEK293) cells were maintained as described previously (18). HEK293 cells stably expressing human TLR4, MD2, and CD14 (293-TLR4 cells) and HEK293 cells stably expressing human TLR2 and CD14 (293-TLR2 cells) were obtained from InvivoGen.

Mice. iNOS-deficient ($iNOS^{-/-}$) mice and endothelial-NOS (eNOS)-deficient ($eNOS^{-/-}$) mice were from The Jackson Laboratories. C57BL/6J control (wild-type) mice were obtained from Japan SLC. All mice were kept under specific pathogen-free conditions. Male mice between 6 and 10 weeks of age were used for all of experiments. All animal protocols were approved by the National Institute for Longevity Sciences Animal Experimentation Committee at the National Center for Geriatrics and Gerontology (Aichi, Japan).

For LPS-induced acute lung injury, anesthetized mice received *Escherichia coli* LPS dissolved in pyrogen-free phosphate-buffered saline (PBS) containing 1 mg/ml Evans Blue intratracheally immediately after mechanical ventilation. After 30 min of administration, lung was excised and then lysed for immunoblot analysis. The febrile responses in mice treated with *E. coli* LPS were tested according to a protocol described previously (45, 49). Mice ($n = 6$) were maintained at a neutral ambient temperature of 31°C and challenged by intraperitoneal (i.p.) injection of 5 mg LPS/kg of body weight dissolved in pyrogen-free PBS. A high dose of LPS (more than 50 mg/kg) was fatal within 90 min in $eNOS^{-/-}$ mice. A colonic thermocouple was inserted and fixed to the base of the tail with adhesive tape. The change in temperature was monitored at 5-min intervals during a period of 120 min after LPS administration. All of the tests were performed at the temperature of 31°C. After 2 h or 12 h of LPS administration, 2 ml of PBS was injected into the abdominal cavity of each mouse. Then, fluids were collected and centrifuged for assessment of cytokine production by an enzyme-linked immunosorbent assay (ELISA). Preparation of peritoneal macrophages was as described previously (28).

Plasmids. The DNA construct encoding 3× Flag-tagged MyD88 fused to the B subunit of the bacterial DNA gyrase (MyD88-GyrB) was as described previously (11). Plasmids encoding human MyD88 and TIRAP were kind gifts from Margaret K. Offermann (Emory University School of Medicine). The cDNAs of N-terminal Flag-tagged and Myc-tagged MyD88, Myc-tagged TIRAP, and IRAK-1 were amplified by PCR and cloned into the pcDNA3.1 vector (Invitrogen). The construct encoding human TLR2 was as described previously (17). Constructs encoding mutated Flag-MyD88 were obtained using a QuikChange II site-directed mutagenesis kit (Stratagene) according to the manufacturer's instructions.

Protein purification. Recombinant Flag-MyD88 proteins were prepared using a FLAG M purification kit (Sigma-Aldrich) from HEK293 cells stably expressing Flag-MyD88 constructs, according to the manufacturer's instructions. Purity of recombinant proteins was confirmed by sodium dodecyl sulfate-polyacrylamide gel electrophoresis (SDS-PAGE), followed by silver staining and immunoblotting with anti-Flag antibody.

Detection of S-nitrosylated proteins. To detect S-nitrosylated MyD88 from lung lysates from wild-type mice and $eNOS^{-/-}$ mice, we referred to the protocol described by Jaffrey et al. (21). Several experiments were performed using a NitroGlo nitrosylation detection kit (PerkinElmer) according to the manufacturer's instructions. Lung lysates from wild-type and $eNOS^{-/-}$ mice were subjected to the biotin switching S-nitrosylation assay, and then biotinylated proteins were purified on streptavidin-agarose. Purified proteins eluted by 2-mercaptoethanol were detected by immunoblotting with anti-MyD88 antibody.

The quantitative measurement of S-nitrosylated recombinant MyD88 by ELISA was performed as follows. Briefly, recombinant Flag-MyD88 (150 μg) was treated with or without SNAP for 30 min at 37°C in the dark. Then, the free sulfides of Flag-MyD88 were blocked with 4 mM methylmethanethionsulfonate for 15 min. After purification by using Micro Bio-Spin chromatography columns (Bio-Rad Laboratories), Flag-MyD88 was reacted with 25 mM ascorbate to be completely denitrosylated. Free sulfides were then labeled with a biotin-conjugated maleimide, using a biotin labeling kit (SH; Dojindo Laboratories) according to the manufacturer's instructions. The diluents of biotinylated Flag-MyD88 proteins dissolved in Tris-buffered saline (pH 7.2) were stabilized in the wells of immobilizer streptavidin plates (Nunc). Flag-MyD88 proteins in the wells were detected by using anti-Flag antibody and a secondary antibody conjugated with horseradish peroxidase. Colorimetric reaction was detected by absorbance on a spectrophotometer at 450 nm. Results were expressed as means ± standard deviations (SD) of three determinations.

Photolysis of S-nitrosylated proteins. Mouse lung lysates were exposed for 3 min to a UV-visible light mercury vapor lamp according to a protocol recently described (8). The samples were then subjected to the biotin switch technique as described above.

Luciferase reporter assay. 293-TLR2 cells were transiently transfected with wild-type MyD88-GyrB or MyD88-GyrB mutants, each with a cysteine residue replaced with a serine residue, together with 50 ng of an NF-κB (5×) luciferase reporter plasmid (pNF-κB-Luc; Stratagene) and 5 ng of an internal control luciferase reporter plasmid (pRL-TK; Promega) and incubated for 16 h. At 6 h before the end of incubation, cells were treated with or without 250 μM SNAP. Cells were then stimulated with 100 ng/ml Pam_3CSK_4 for 6 h. HEK293 cells stably expressing MyD88-GyrB were transfected with pNF-κB-Luc and pRL-TK. After 24 h of incubation, cells were stimulated with coumermycin A in the presence and absence of 250 μM SNAP. The dual luciferase activity was measured as described previously (19).

Immunoblot analysis of IRAK-1 and IκBα. HAECs were stimulated with 10 ng/ml of LPS for 0 to 90 min. HEK293 cells stably expressing MyD88-GyrB were stimulated with 1 μM coumermycin for 20 min. Cells were lysed in the presence of protease inhibitor and phosphatase inhibitor cocktails (Roche) at 4°C. Cell lysates or lysates from the mouse lungs were separated by SDS-PAGE, followed by immunoblot analyses using anti-IRAK-1, anti-IκBα, and phosphorylation-specific anti-IκBα (Ser32/Ser36) antibodies (Cell Signaling Technology).

RNA extraction and reverse transcription-PCR. Total RNA was isolated from mouse peritoneal macrophages stimulated with 100 ng/ml LPS and 10 ng/ml gamma interferon, and transcripts were quantified by real-time quantitative reverse transcription-PCR on a LightCycler ST300 system (Roche). All values were normalized to the level of β-actin mRNA. The primer sets used are as follows: for mouse macrophage inflammatory protein 2 (MIP-2), 5′-ATCCAGAGCTTGAGTGTGACGC-3′ (sense) and 5′-AAGGCAAACTTTTTGACCGAA-3′ (antisense); for mouse IL-6, 5′-CCACGGCCTTCCCTAC-3′ (sense) and 5′-AGTGCATCATCGTTGTTC-3′ (antisense); and for mouse β-actin, 5′-AAATCGTGCGTGACATCAAA-3′ (sense) and 5′-AAGGAAGGCTGGAAAAGAGC-3′ (antisense).

Cytokine ELISA. Concentrations of human IL-8, mouse MIP-2, and mouse IL-6 were determined using a Cytoset ELISA kit (Biosource) according to the manufacturer's instructions.

Subcellular fractionation. Subcellular fractionation of HEK293 cells stably expressing Flag-MyD88 and 293-TLR4 cells stably expressing Flag-MyD88-GyrB

MOLECULAR AND CELLULAR BIOLOGY, Feb. 2008, p. 1338–1347 Vol. 28, No. 4
0270-7306/08/$08.00+0 doi:10.1128/MCB.01412-07

Regulation of MyD88-Dependent Signaling Events by S Nitrosylation Retards Toll-Like Receptor Signal Transduction and Initiation of Acute-Phase Immune Responses[▽]

Takeshi Into,[1]* Megumi Inomata,[1] Misako Nakashima,[1] Ken-ichiro Shibata,[2] Hans Häcker,[3] and Kenji Matsushita[1]

Department of Oral Disease Research, National Institute for Longevity Sciences, National Center for Geriatrics and Gerontology, 36-3, Gengo, Morioka, Obu, Aichi 474-8522, Japan[1]; Laboratory of Oral Molecular Microbiology, Department of Oral Pathobiological Science, Hokkaido University Graduate School of Dental Medicine, Sapporo 060-8586, Japan[2]; and Department of Infectious Diseases, St. Jude Children's Research Hospital, 332 North Lauderdale Street, Memphis, Tennessee 38105[3]

Received 7 August 2007/Returned for modification 23 September 2007/Accepted 28 November 2007

Nitric oxide (NO) has been thought to regulate the immune system through S nitrosylation of the transcriptional factor NF-κB. However, regulatory effects of NO on innate immune responses are unclear. Here, we report that NO has a capability to control Toll-like receptor-mediated signaling through S nitrosylation. We found that the adaptor protein MyD88 was primarily S nitrosylated, depending on the presence of endothelial NO synthase (eNOS). S nitrosylation at a particular cysteine residue within the TIR domain of MyD88 resulted in slight reduction of the NF-κB-activating property. This modification could be restored by the antioxidant glutathione. Through S nitrosylation, NO could negatively regulate the multiple steps of MyD88 functioning, including translocation to the cell membrane after LPS stimulation, interaction with TIRAP, binding to TRAF6, and induction of IκBα phosphorylation. Interestingly, glutathione could reversely neutralize such NO-derived effects. We also found that an acute febrile response to LPS was precipitated in eNOS-deficient mice, indicating that eNOS-derived NO exerts an initial suppressive effect on inflammatory processes. Thus, NO has a potential to retard induction of MyD88-dependent signaling events through the reversible and oxidative modification by NO, by which precipitous signaling reactions are relieved. Such an effect may reflect appropriate regulation of the acute-phase inflammatory responses in living organisms.

It is increasingly becoming evident that nitric oxide (NO) regulates a broad spectrum of protein functions through S nitrosylation, a posttranscriptional modification that forms *S*-nitrosothiol by covalent addition to cysteine residues of an NO moiety (14, 42, 43). Through S nitrosylation, NO is thought to exert a physiological inhibitory effect on nuclear factor κB (NF-κB) (25, 32, 33, 39), the major transcriptional factor family deeply associated with regulation of the immune system through transcription of a wide range of genes, including cytokines, adhesion molecules, antimicrobial molecules, and antiapoptotic molecules (10, 13, 24). S nitrosylation of NF-κB inhibits its DNA binding, promoter activity, and subsequent transcription (25, 33). It has been known that S nitrosylation targets a particular cysteine residue of the NF-κB p50 and p65 subunits located in the N-terminal DNA binding loop within the Rel homology domain (25, 32, 33). This residue is conserved in other NF-κB subunits, including p52, p100, p105, and c-Rel, and other Rel homology domain-containing molecules. Upstream of NF-κB, IκB kinase β (IKKβ), a catalytic subunit of the IκB (inhibitor of NF-κB) kinase complex, also undergoes S nitrosylation, resulting in reduction of its kinase function on phosphorylation of IκB (39). Such reduction of the IKKβ function leads to reduced IκB ubiquitinylation and proteasomal degradation, resulting in NF-κB inhibition (14, 32, 39).

Toll-like receptors (TLRs) are the central innate immune sensors for a broad array of pathogen-associated molecular patterns, ranging from bacterial constituents to viral genomes (2, 35). TLRs initiate early processes of proinflammatory immune responses that help to strengthen the processes of innate and adaptive immunity (2, 20), in which NF-κB plays many important roles (13, 24). TLRs utilize MyD88, a Toll/interleukin-1 receptor (IL-1R) homology (TIR) domain-containing adaptor molecule, to activate the NF-κB pathway through IL-1R-associated kinases (IRAKs) and tumor necrosis factor (TNF) receptor-associated factor 6 (TRAF6) (1). It has been thought that TLR agonistic molecules, such as lipopolysaccharide (LPS), can regulate NO generation through upregulation of expression of all NO synthase (NOS) isoforms through NF-κB activation (4, 9, 32). TLR stimulation can directly activate an antimicrobial property through inducible NOS (iNOS) expression and NO generation in macrophages (46). NO generation is a general feature of immune cells, including neutrophils, monocytes, macrophages, dendritic cells, and NK cells, as well as other cells, including endothelial cells, epithelial cells, and fibroblasts (4), all of which express multiple members of the TLR family. However, it has remained obscure whether generated NO exerts any regulatory effects on TLR signaling or subsequent processes of innate immune responses.

There has been an accumulation of biochemical evidence indicating that TLR signaling components, including IKKβ

* Corresponding author. Mailing address: Section of Oral Infection Control, Department of Oral Disease Research, National Institute for Longevity Sciences, National Center for Geriatrics and Gerontology, 36-3 Gengo, Morioka, Obu, Aichi 474-8522, Japan. Phone: 81-562-44-5651, ext. 5064. Fax: 81-562-46-8684. E-mail: into@nils.go.jp.

▽ Published ahead of print on 17 December 2007.

was performed using a ProteoExtract subcellular proteome extraction kit (Calbiochem) according to the manufacturer's instructions. This kit enables extraction of different subcellular fractions of the cytoplasm, plasma membrane, nuclei, and cytoskeleton from mammalian cells. 293-TLR4 cells stably expressing Flag-MyD88-GyrB were maintained in serum-free Dulbecco's modified Eagle's medium containing 5% PANEXIN H cell growth supplement (PAN Biotech GmbH) to avoid nonspecific cell activation by animal serum components. The whole-cell lysate was obtained using NuPAGE LDS sample buffer containing 2-mercaptoethanol. Each fraction was mixed with NuPAGE LDS sample buffer and boiled for 5 min, followed by SDS-PAGE and immunoblot analyses using anti-Flag (Sigma), anti-MyD88 (Santa Cruz Biotechnology), anti-IRAK-1, and anti-vimentin (BD Biosciences) antibodies.

Blue native PAGE and immunoprecipitation. HEK293 cells stably expressing Flag-MyD88 were treated with SNAP for 1 h, washed twice with PBS, and lysed with HEPES buffer (pH 7.2) containing 1% Triton X-100, 1% Nonidet-P40, and proteinase inhibitor cocktail (Roche). Cell lysates were separated by blue native PAGE according to the protocol provided by Invitrogen and then immunoblotted with anti-Flag antibody. HEK293 cells transiently transfected combinatorially with Flag-MyD88 and Myc-TIRAP or Flag-MyD88 and IRAK-1 were treated with GSNO or GSH for 1 h. HEK293 cells stably expressing 3× Flag-MyD88-GyrB were stimulated with 1 μM coumermycin A for 20 min. Cells were lysed with HEPES buffer (pH 7.2) containing 1% Triton X-100 and proteinase inhibitor cocktail (Roche). Clarified cell lysates were immunoprecipitated with anti-Flag antibody, followed by immunoblot analysis using anti-Flag, anti-Myc, and anti-TRAF6 (StressGen) antibodies. All experiments were performed at least three times, and representative results are shown.

Immunofluorescent cell staining. HAECs were fixed at −20°C with methanol, and double immunostaining was then carried out with anti-β-actin monoclonal antibody (Santa Cruz Biotechnology) and Alexa 488-conjugated immunoglobulin G secondary antibody (Invitrogen) and then with anti-MyD88 rabbit polyclonal antibody (Santa Cruz Biotechnology) and Alexa 564-conjugated immunoglobulin G secondary antibody (Invitrogen). Cell nuclei were also stained with 2.5 μg/ml of Hoechst 33342 for 30 min.

Statistical analysis. Probability (*P*) values were calculated by Student's *t* test and analysis of variance and were considered significant at 0.05 or 0.01.

RESULTS

TLR signaling components are S nitrosylated in vivo. To examine whether TLR signal components are physiologically S nitrosylated in vivo, we detected S-nitrosylated proteins in the lung lysates from wild-type and eNOS$^{-/-}$ mice by utilizing the biotin switch method (21). Interestingly, this method facilitated the detection of MyD88 as an S-nitrosylated protein (Fig. 1A). To exclude the possibility that the detection of S-nitrosylated MyD88 is an experimental artifact, we utilized the biotin switch method combined with photolysis of S nitrosylation, which has recently been reported as a useful method for confirming the specificity of S nitrosylation (8). The detectable S-nitrosylated MyD88 protein was reduced after exposure of the samples to a UV lamp (Fig. 1B), suggesting that the result is not false positive. Thus, our result at least suggests that MyD88 is potentially S nitrosylated in addition to other signaling molecules, including NF-κBs, ASK1, and caspase-1.

We further examined the details of S-nitrosylated MyD88 in vitro by utilizing a quantitative method for detecting S nitrosylation of recombinant proteins. We could detect S nitrosylation of recombinant MyD88, which increased, accompanied by an increase in the concentration of the NO donor SNAP (Fig. 1C). It has been known that S-nitrosylated proteins are reversibly denitrosylated by antioxidants or oxidoreductases, by which substantial protein functions are restored (14, 42). Indeed, the detectable S-nitrosylated MyD88 protein was reduced when the NO donor-treated protein was reacted with ascorbate, $HgCl_2$, or GSH (Fig. 1C). We further determined the site of S nitrosylation because the modification is effected toward particular cysteine residues (14). Mammalian MyD88 contains a total of nine cysteine residues: one in a short linker region and the other eight in the TIR domain (Fig. 1D). These residues are thought not to be involved in the formation of intramolecular disulfide bonds. Among vertebrates, all cysteine residues are highly conserved (data not shown). We prepared recombinant MyD88 proteins of nine individual mutants, each with one of the nine cysteine residues replaced with a serine residue. We found that the degrees of S nitrosylation of Cys113 and Cys216 were significantly reduced compared with those of wild-type MyD88 (Fig. 1E). These cysteine residues partially fulfill the predictive site of the S nitrosylation "acid-base motif" that comprises flanking acidic and basic residues (14) (Fig. 1F). Interestingly, the cysteine residue equivalent of Cys216 is conserved even in invertebrates, while others are not (data not shown). Among other TIR domain-containing adaptor molecules, only TIRAP and SIGIRR have a cysteine residue corresponding to the position of Cys216 (Fig. 1G).

To determine the requirement of cysteine residues for functioning of MyD88, we utilized MyD88 fused to the B subunit of the bacterial DNA gyrase (MyD88-GyrB). The *Streptomyces*-derived bivalent antibiotic coumermycin binds GyrB with a stoichiometry of 1:2, acting as a natural dimerizer of GyrB (7). Although overexpressed MyD88 is known to reveal TLR stimulation-independent nonspecific activation of downstream signaling through self-dimerization (11, 36), MyD88-GyrB does not reveal such nonspecific activation unless cells are exposed to TLR stimulation or coumermycin treatment (11). We prepared GyrB-fused wild-type MyD88 and MyD88 mutants, each with one of the nine cysteine residues replaced with a serine residue, and examined the NF-κB-activating properties in the TLR2 ligand Pam_3CSK_4-stimulated HEK293 cells stably expressing TLR2. None of the cysteine replacement mutants abrogated the NF-κB-activating property of MyD88 (Fig. 1H). However, the Cys216Ser mutant significantly increased the activity compared with that of wild-type MyD88 (Fig. 1H). Additionally, similar results were found in the cells treated with SNAP (Fig. 1H). Thus, it is possible that Cys216 of MyD88 mediates the suppressive effect of NO.

S nitrosylation alters MyD88-mediated signaling events. We next explored how S nitrosylation of signaling components alters TLR signaling events. To examine this in vivo, we utilized an animal model of acute lung injury induced by intratracheal administration of LPS. We investigated degradation of IRAK-1 and IκBα, hallmarks of MyD88-dependent and IKKβ-dependent signaling events, in the lungs 30 min after LPS administration. Interestingly, degradation of IRAK-1 and IκBα was apparently promoted in eNOS$^{-/-}$ mice compared with that in wild-type mice (Fig. 2A). We also examined whether NO alters degradation of IRAK-1 and IκBα in cultivated vascular endothelial cells. In HAECs, LPS induced degradation of IRAK-1 and IκBα within 30 min after stimulation (Fig. 2B). Degradation of IRAK-1 and IκBα was promoted and occurred within 15 min after stimulation when endogenous NO was predepleted by the L-arginine analog L-NMMA (Fig. 2B). In addition, IRAK-1 degradation was also promoted when confluent HAECs were maintained in culture media without the eNOS activator vascular endothelial growth factor or the phosphatidylinositol 3-kinase inhibitor LY294002 (data not shown). In contrast to these results, degradation was delayed

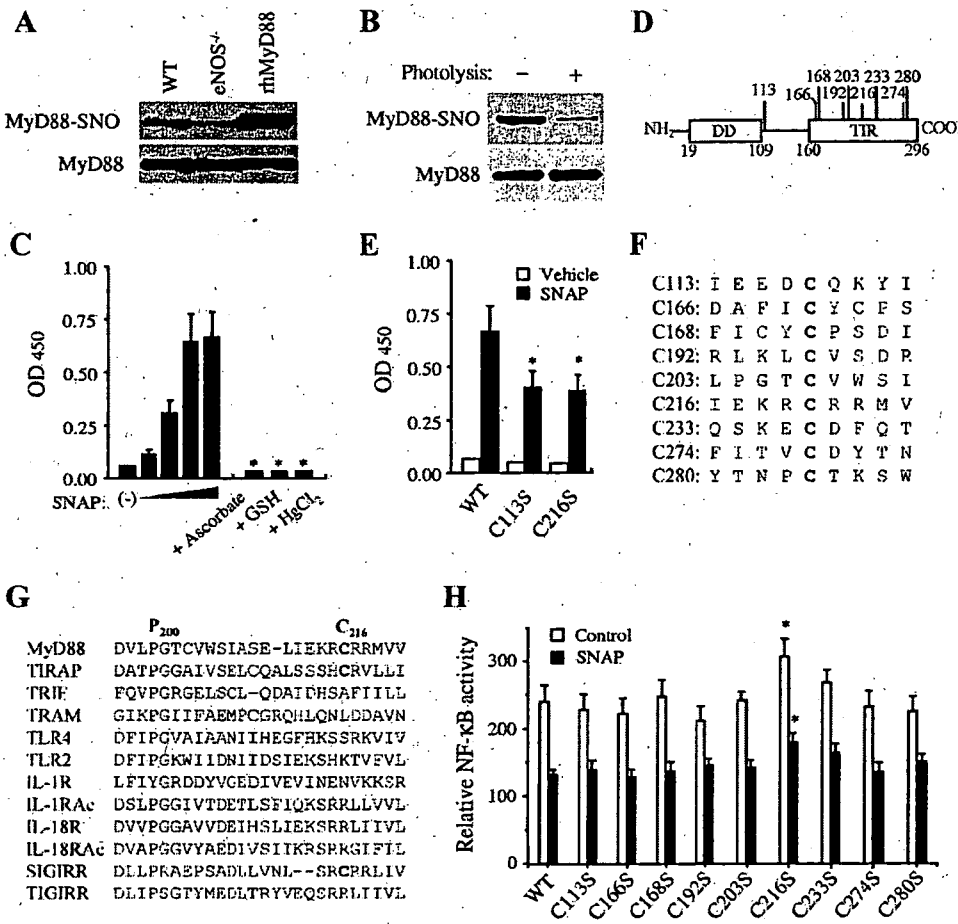

FIG. 1. S nitrosylaton of MyD88. (A) Lung lysates from wild-type (WT) and eNOS$^{-/-}$ mice and SNAP-treated recombinant human MyD88 (rhMyD88) were subjected to the biotin switching S-nitrosylation assay, and then biotinylated proteins were purified on streptavidin-agarose. Purified proteins were detected by immunoblotting with anti-MyD88 antibody (upper). MyD88 proteins in lung lysates and rhMyD88 were also shown as loading controls (lower). (B) Mouse lung lysates were exposed for 3 min to a UV-visible light mercury vapor lamp. The samples were then subjected to the biotin switch method. (C) A recombinant Flag-MyD88 protein was treated with or without SNAP (100, 200, 500, and 1,000 μM) for 30 min. For the denitrosylation study, SNAP-treated proteins were incubated with 1 mM ascorbic acid, 1 mM GSH, or 1 mM $HgCl_2$ for 5 min before the blockade of free thiols by methylmethanethionsulfonate. Then, S-nitrosylated residues of MyD88 were switched into biotins and proteins were fixed on streptavidin-coated plates, followed by ELISA with anti-Flag antibody. Each value is the mean ± SD (n = 3). See text for details. (*, $P < 0.01$ for comparison with the group of 500 μM SNAP). (D) Schematic of human MyD88. (E) Recombinant Flag-MyD88 wild-type proteins and mutants with each cysteine residue replaced with a serine residue were treated with or without 500 μM SNAP for 30 min. Then, S-nitrosylated MyD88 fixed on streptavidin-coated plates was detected by ELISA using anti-Flag antibody. Each value is the mean ± SD (n = 3). See text for details. (*, $P < 0.01$ for comparison with the wild-type group). (F) Sequence alignment of the region around nine cysteine residues of MyD88. (G) Sequence alignment of human TIR domain-containing molecules. The regions corresponding to that around the residues of Pro200, a critical residue for TIR-TIR interaction, and Cys216 of MyD88 are shown. (H) HEK293 cells stably expressing TLR2 were transiently transfected with GyrB-fused wild-type MyD88 or mutant MyD88 with each cysteine residue replaced with a serine residue together with the NF-κB-driven luciferase gene and incubated for 16 h. At 6 h before the end of incubation, cells were treated with 200 μM SNAP. Cells were stimulated with 100 ng/ml Pam_3CSK_4 for 6 h, and then luciferase activity was measured. Each value is the mean ± SD (n = 3). (*, $P < 0.05$ for comparison with the wild-type group).

and residual proteins were observed even at 45 min after stimulation when cells were pretreated with SNAP (Fig. 2B). The effect of NO was not altered in the presence of the guanylate cyclase inhibitor ODQ or the cyclic-GMP-dependent protein kinase inhibitor KT5823 (data not shown). Notably, LPS-induced degradation of IRAK-1 and IκBα in HAECs was prevented by the irreversible thiol modification by *N*-ethylmaleimide (Fig. 2C), implying that the effect of NO on the signaling events depends on modification of cysteine residues.

To test whether NO alters the MyD88-dependent signal events, we utilized the MyD88-GyrB construct. Under coumermycin treatment of cells stably expressing MyD88-GyrB, MyD88-GyrB undergoes dimerization and mimics TLR-triggered typical MyD88-dependent functions, such as the activation of MAPKs and IKKs and secretion of proinflammatory cytokines (11). We found that coumermycin-dependent induction of NF-κB activation in HEK293 cells was suppressed by pretreatment with cells with NO donors (Fig. 3A). Coumermycin could induce phosphorylation of IκBα at Ser32 and Ser36, the target residues of IKKβ involved in degradation of IκBα (51), but SNAP pretreatment could suppress induction of the response (Fig. 3B). SNAP also suppressed coumermycin-induced phos-

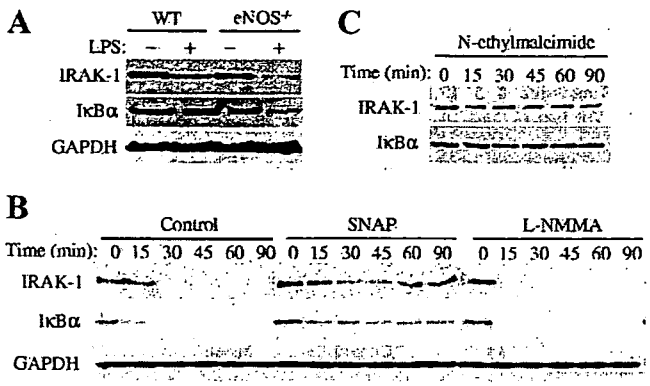

FIG. 2. NO suppresses LPS-induced degradation of IRAK-1 and IκBα. (A) Anesthetized wild-type (WT) and eNOS$^{-/-}$ mice intratracheally received *E. coli* LPS and mechanical ventilation. After 30 min of administration, lung was excised and then lysed for immunoblotting with anti-IRAK-1, anti-IκBα, and anti-GAPDH antibodies. (B) HAECs pretreated with 1 mM L-NMMA for 12 h or 0.25 mM SNAP for 1 h were stimulated with 10 ng/ml *E. coli* LPS for the indicated periods. The expression levels of IRAK-1 and IκBα were determined by immunoblot analysis. (C) HAECs pretreated with 0.1 mM *N*-ethylmaleimide for 10 min were stimulated with 10 ng/ml *E. coli* LPS for the indicated periods. The expression levels of IRAK-1 and IκBα were determined by immunoblot analysis.

phorylation of MAPKs (data not shown). The coumermycin-dependent dimerization of MyD88-GyrB induced interaction with TRAF6, consistent with a previous study (10), and we found that this interaction was reduced by SNAP treatment (Fig. 3C).

We found that NO and alteration of Cys113 and Cys216 residues of MyD88 did not alter the interaction of overexpressed MyD88 with IRAK-1 in HEK293 cells (Fig. 3D). However, NO clearly attenuated TLR4 stimulus (LPS)-dependent induction of MyD88–IRAK-1 interaction (Fig. 3E), suggesting that NO targets upstream signaling events of IRAK-1. It has been known that the recruitment of MyD88 to TLR2 or TLR4 is mediated by binding of the sorting adaptor TIRAP to the membrane phosphatidylinositol 4,5-bisphosphate, followed by interaction of MyD88 with TIRAP through TIR-TIR interaction (23). We examined whether NO affects the interaction of MyD88 with TIRAP. Overexpressed MyD88 interacted with TIRAP in HEK293 cells (Fig. 3F). We found that treatment of the cells with the NO donor GSNO attenuated the interaction (Fig. 3F). We further investigated whether S nitrosylation of residues 113 and 216 is involved in MyD88-TIRAP interaction. Alteration of Cys residues did not affect the interaction (Fig. 3G). However, SNAP-induced attenuation of the interaction was reduced in the Cys216 mutant (Fig. 3G).

In HAECs, MyD88 was enriched with filamentous cytoskeletal structures and partly colocalized with β-actin (Fig. 4A). Additionally, a large part of MyD88 stably expressed in HEK293 cells was found in the cytoskeletal fraction (Fig. 4B). These findings are consistent with results of a previous study showing that MyD88 associates with β-actin in HeLa cells (22). Cytoskeletal MyD88 was separated from IRAK-1, which was found only in the cytoplasm (Fig. 4B), suggesting that MyD88 is maintained as an inactive state in cytoskeleton. We found that SNAP treatment altered such cytoskeletal localization of MyD88 into the cytoplasm (Fig. 4C). We further investigated the subcellular localization of MyD88 after TLR4 stimulation in 293-TLR4/MD2-CD14 cells stably expressing Flag-MyD88-GyrB. After LPS treatment, a part of MyD88 was transported to the cytoplasmic membrane from the cytoskeleton (Fig. 4D). However, SNAP treatment retarded such LPS-induced transportation of MyD88 (Fig. 4D). Although native PAGE analysis revealed that MyD88 formed a protein complex (more than 480 kDa) in HEK293 cells, SNAP treatment resulted in reduction in the size of the complex to approximately 450 kDa or 250 kDa, accompanied by an increase in concentration (Fig. 4E). Moreover, higher concentrations of SNAP further altered the complex to render a monomer (approximately 35 kDa) (Fig. 4E), implying disruption of functional MyD88 protein complex by NO.

Thus, NO has a capability to obstruct the MyD88 signing pathway through disruption of the multiple steps of protein interactions.

NO reversibly suppresses the MyD88 signaling events. S-nitrosylated proteins are known to undergo denitrosylation, by which regulatory effects of NO are conferred to control protein functions. We therefore investigated how S nitrosylation and denitrosylation affect MyD88-mediated signaling events. For this purpose, we utilized GSH because GSH had a capability to denitrosylate MyD88 (Fig. 1C). We found that GSH restored NO-induced impaired interaction of MyD88 with TIRAP (Fig. 4F). Furthermore, the NO-induced cytoplasmic localization of cytoskeletal MyD88 was restored by treatment of the cells with GSH (Fig. 4G). Thus, these results suggest that S nitrosylation alters the MyD88 pathway, and antioxidants or oxidoreductases restore such NO-derived actions, probably through denitrosylation.

NO reversibly suppresses TLR-mediated cellular responses. HAECs responded to multiple bacterial TLR agonistic molecules, Pam_3CSK_4 (for TLR1/TLR2), MALP-2 (for TLR2/TLR6), LPS (for TLR4), flagellin (for TLR5), and IL-1β, all of which are known to activate MyD88-dependnet signaling to induce production of the NF-κB-driven chemokine IL-8 after stimulation for 3 h (Fig. 5A). Predepletion of endogenous NO by L-NMMA resulted in a significant increase in IL-8 production induced by each stimulator (Fig. 5A), indicating that endogenous NO has a suppressive effect on the TLR-mediated cellular response. Furthermore, IL-8 production by each stimulator was suppressed in the presence of SNAP (Fig. 5A). The effect of NO donors was not altered in the presence of ODQ or KT5823 (data not shown). We investigated whether such a suppressive effect of NO can be restored because S nitrosylation is a reversible protein modification. However, it is difficult to examine the effects of antioxidants or oxidoreductases because the TLR signaling pathway is greatly affected by reactive oxygen species generated from NADPH oxidases (27, 34, 48). Indeed, treatment of cells with ascorbic acid, GSH, NAC, or the NADPH oxidase inhibitor DPI greatly impaired LPS-induced IL-8 production in HAECs (Fig. 5B). We therefore attempted to address whether the effect of NO is transient or persistent. For this purpose, HAECs were pretreated with SNAP for 1 h and washed two times to remove the NO donor. Then, at various times afterwards, the cells were stimulated with LPS and IL-8 production was measured. NO suppression of IL-8 production was gradually neutralized or restored in a

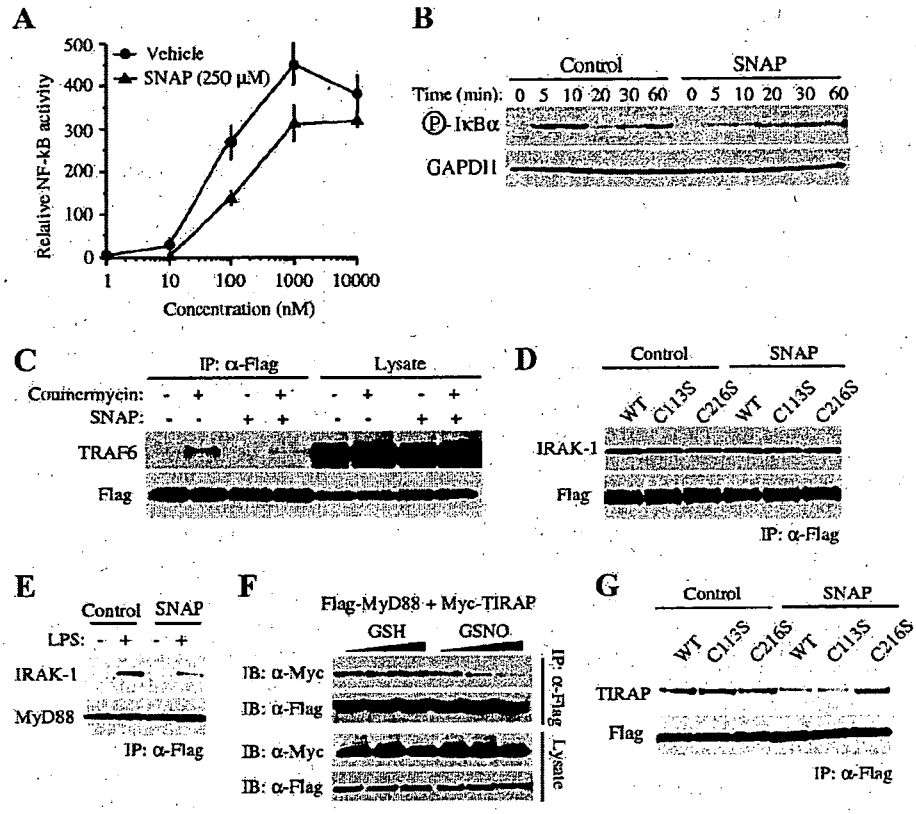

FIG. 3. Effects of NO on TLR-mediated signaling events. (A) HEK293 cells stably expressing MyD88-GyrB were transiently transfected with an NF-κB-driven luciferase gene and incubated for 24 h. Cells were pretreated with or without 0.25 mM SNAP for 1 h and then treated with 1 μM coumermycin for 3 h. Then, luciferase activity was measured. Each value is the mean ± SD (n = 3). (B) HEK293 cells stably expressing MyD88-GyrB were pretreated with or without 0.25 mM SNAP for 1 h and then treated with 1 μM coumermycin for the indicated periods. The phosphorylation of IκBα at Ser32/Ser36 was detected by immunoblot analysis. (C) HEK293 cells stably expressing MyD88-GyrB were pretreated with or without 0.25 mM SNAP for 1 h and then treated with 1 μM coumermycin for 20 min. Then, cell lysates were immunoprecipitated (IP) with anti-Flag antibody, followed by immunoblotting with anti-Flag and anti-TRAF6 antibodies. (D) HEK293 cells transiently expressing Flag-tagged wild-type (WT) or Cys residue (113 or 216) replacement MyD88 together with IRAK-1 were treated with 500 μM SNAP for 1 h. Then, cell lysates were immunoprecipitated with anti-Flag antibody, followed by immunoblotting with anti-Flag and anti-IRAK-1 antibodies. (E) 293-TLR4/MD2-CD14 cells stably expressing Flag-MyD88-GyrB were treated with or without 500 μM SNAP for 1 h and then stimulated with 100 ng/ml LPS for 20 min. Then, cell lysates were immunoprecipitated with anti-Flag antibody, followed by immunoblotting with anti-IRAK-1 and anti-Flag antibodies. (F) HEK293 cells transiently expressing Flag-tagged MyD88 together with Myc-tagged TIRAP were treated with GSH or GSNO (0, 100, and 500 μM) for 1 h. Then, cell lysates were immunoprecipitated with anti-Flag antibody, followed by immunoblotting (IB) with anti-Flag and anti-Myc antibodies. (G) HEK293 cells transiently expressing Flag-tagged wild-type or Cys residue (113 or 216) replacement MyD88 together with Myc-tagged TIRAP were treated with 500 μM SNAP for 1 h. Then, cell lysates were immunoprecipitated with anti-Flag antibody, followed by immunoblotting with anti-Flag and anti-IRAK-1 antibodies.

time-dependent manner, although the restrictive effect continues for several hours (Fig. 5C).

NO suppresses acute-phase immune responses to LPS in vivo. To explore how NO regulation of MyD88-dependent signaling reflects innate immune or proinflammatory responses in vivo, we utilized a popular animal model of sepsis induced by i.p. administration of LPS. We first investigated the cytokine responses as the major hallmark of innate immune responses. MIP-2 is known as one of the early LPS-responsive genes, the mRNA expression of which indeed showed a rapid rise and reached a peak within 1 h after LPS stimulation in mouse peritoneal macrophages (Fig. 6A). In contrast, IL-6 is known as a late LPS-responsive gene, the expression of which showed a gradual rise and reached a peak more than 4 h after stimulation (Fig. 6A). We determined the amounts of MIP-2 and IL-6 produced in the abdominal cavity 2 h after LPS administration in wild-type, eNOS$^{-/-}$, and iNOS$^{-/-}$ mice. Interestingly, eNOS$^{-/-}$ mice exhibited the most intensive production of MIP-2 (Fig. 6B). On the other hand, the most prominent production of IL-6 was observed in iNOS$^{-/-}$ mice (Fig. 6C). In contrast to these results, there was no significant difference in the amounts of MIP-2 and IL-6 production when the fluids were collected 12 h after LPS administration (data not shown). Thus, eNOS and iNOS at least exert a suppressive effect on early cytokine responses in vivo.

We further examined LPS-induced febrile response as a hallmark of acute-phase responses of inflammation. LPS is known to act as a pyrogen to induce TLR4-dependnet polyphasic fever (44). The major initiator of LPS fever is generated prostaglandin E2, which stimulates thermoregulatory neurons and elevates body core temperature (3). LPS can directly induce prostaglandin E2 generation through the MyD88-dependent signaling pathway (47). The first-phase febrile response in eNOS$^{-/-}$ mice occurred significantly earlier than that in wild-

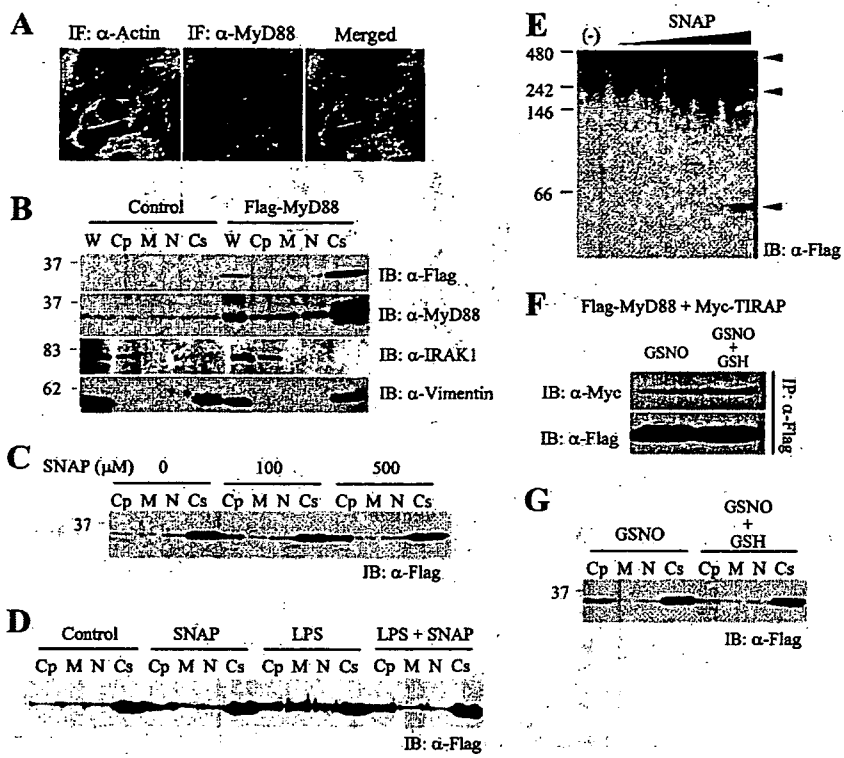

FIG. 4. Reverse of the suppressive effect of NO by GSH. (A) HAECs were fixed and stained immunofluorescently (IF) with anti-β-actin antibody (green, left), anti-MyD88 antibody (red, middle), and Höechst33342 (blue, right). (B) Parental HEK293 cells and HEK293 cells stably expressing Flag-MyD88 were fractionated into the cytoplasm (Cp), cytoplasmic membrane (M), nucleus (N), and cytoskeleton (Cs). Whole-cell lysates (W) were also obtained. The fractions were assessed by immunoblotting (IB) with anti-Flag, anti-MyD88, anti-IRAK-1, and anti-vimentin antibodies. (C) HEK293 cells stably expressing Flag-MyD88 were treated with the indicated concentration of SNAP for 1 h and fractionated into each fraction. The fractions were assessed by immunoblotting with anti-Flag antibody. (D) 293-TLR4/MD2-CD14 cells stably expressing Flag-MyD88-GyrB were treated with or without 500μM SNAP for 1 h and then stimulated with 100 ng/ml LPS for 20 min. Cells were then fractionated into each fraction. The fractions were assessed by immunoblotting with anti-Flag antibody. (E) HEK293 cells stably expressing Flag-MyD88 were treated with or without SNAP (10, 50, 125, 250, and 500 μM) for 1 h. Then, cell lysates were assessed by blue native PAGE and immunoblotting with anti-Flag antibody. (F) HEK293 cells transiently expressing Flag-MyD88 and Myc-tagged TIRAP were treated with 500 μM GSNO for 1 h and then with or without 500 μM GSH for 15 min. Then, cell lysates were immunoprecipitated with anti-Flag antibody, followed by immunoblotting with anti-Flag and anti-Myc antibodies. (G) HEK293 cells stably expressing Flag-MyD88 were treated with the 500 μM GSNO for 1 h and then with or without 500 μM GSH for 15 min. The cells were fractionated into each fraction, followed by immunoblotting with anti-Flag antibody.

type or iNOS$^{-/-}$ mice (Fig. 6D), indicating that NO from eNOS suppresses the initiation of the response. However, eNOS deficiency did not alter the magnitude of febrile response compared with that for wild-type mice, suggesting that the suppressive effect of NO is not persistent. On the other hand, a transient decrease in fever was found in wild-type and eNOS$^{-/-}$ mice at about 70 min after LPS administration but not in iNOS$^{-/-}$ mice (Fig. 6D), indicating that NO from iNOS suppresses promotion of the response. Thus, these results suggest that NO generated from eNOS and iNOS exerts a suppressive effect on acute-phase inflammatory responses to LPS in vivo, probably through S nitrosylation.

DISCUSSION

Our findings imply that MyD88-dependent signaling events are affected by S nitrosylation, by which innate immune signal transduction might be reduced in living organisms. The effect of NO is transient and is restored by antioxidants or oxidoreductases, in which protein denitrosylation plays an important role. Although the physiological significance of such regulation of TLR signal transduction is unsettled, NO is likely to retard signaling cascades through S nitrosylation, by which rapid and precipitous signaling reactions may be initially or inductively relieved. Such an effect may reflect an adequate regulation of acute-phase inflammatory responses, leading to limitation of the degree of inflammation and resolution of inflammation.

We found that the suppressive effect of NO on TLR-mediated cellular responses was transient and degraded in a time-dependent manner (Fig. 5C). The specificity of NO regulation may be conferred by the spatial regulation of S nitrosylation within or between proteins and the stimulus-coupled temporal regulation through denitrosylation (14). Signal transduction by ligand-receptor interactions is thought to trigger denitrosylation, restoring substantial protein functions. For example, reduction of the functions of caspase-3 and IKKβ by S nitrosylation is restored by FasL-Fas interaction and TNF-α–TNFR interaction, respectively (30, 39). Thus, it is possible that TLR ligation-dependent protein denitrosylation also facilitates the restoration of NO suppression although the mechanism of denitrosylation has been poorly studied. Protein denitrosyla-

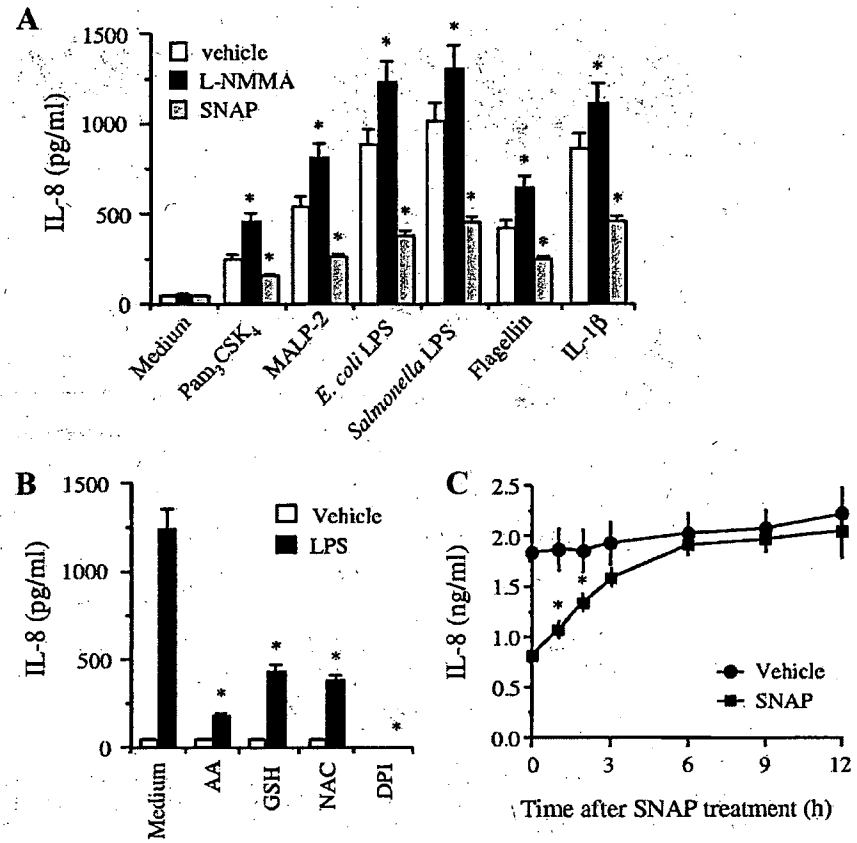

FIG. 5. NO reversibly suppresses TLR-mediated cellular responses. (A) HAECs pretreated with 1 mM L-NMMA for 12 h or 0.25 mM SNAP for 1 h were stimulated with 1 μg/ml Pam_3CSK_4, 100 nM MALP-2, 10 ng/ml *E. coli* LPS, 10 ng/ml *Salmonella* LPS, 5 μg/ml flagellin, and 10 ng/ml IL-1β for 3 h. Then, production of IL-8 was determined by ELISA. Each value is the mean ± SD ($n = 3$). *, $P < 0.01$ for comparison with the vehicle group. (B) HAECs were stimulated with 10 ng/ml *E. coli* LPS for 3 h in the presence or absence of 1 mM ascorbic acid (AA), 1 mM GSH, 1 mM NAC, or 20 μM DPI. Then production of IL-8 was determined by ELISA. Each value is the mean ± SD ($n = 3$). (*, $P < 0.01$ for comparison with the vehicle group). (C) HAECs were treated with 0.25 mM SNAP for 1 h and then at various times afterwards stimulated with 10 ng/ml *E. coli* LPS for 3 h. Then, production of IL-8 was determined by ELISA. Each value is the mean ± SD ($n = 3$). (*, $P < 0.01$ for comparison with the vehicle group).

tion is catalyzed by antioxidants or oxidoreductases, including ascorbic acid, thioredoxin-thioredoxin reductase, superoxide dismutase GSH, and GSNO reductase (14, 15, 50, 53). S-nitrosylated MyD88 can be denitrosylated in the presence of ascorbic acid and GSH in vitro (Fig. 1C). Although it is still unclear how TLR ligation activates cellular redox activity, LPS has a potential to activate cellular redox activity and transition of GSH into GSNO (41). More details of TLR-mediated protein S nitrosylation and denitrosylation should be investigated in future studies.

TLR ligation can initiate recruitment of MyD88 to the receptor complex through TIR-TIR interaction. In the case of TLR2 and TLR4, the sorting adaptor TIRAP is essentially required to recruit MyD88 (23). MyD88 then dissociates from the receptor complex and recruits IRAK-1 (and IRAK-4) through death domain (DD)-DD interaction, inducing TRAF6-mediated signaling events and ubiquitin ligation to IRAK-1 or IκBα, followed by proteasomal degradation (1). Nevertheless, how MyD88 can be initially controlled to be recruited to TLRs has remained unclear. We found that a large part of cellular MyD88 existed in the cytoskeleton and associated with β-actin (Fig. 4A and B), wherein MyD88 formed a complex dissociated from IRAK-1 (Fig. 4B). Our finding suggests that MyD88 preferentially interacts with the cytoskeleton as an inactive form, followed by release into the cytoplasm and recruitment to TLRs after ligation-dependent actin rearrangement. Indeed, inhibition of actin rearrangement by cytochalasin D suppresses LPS-induced signal transduction and cytokine production (5). In addition, cytochalasin D also alters TIRAP recruitment to the cytoplasmic membrane (23). NO restriction of MyD88 function may be achieved through disruption of the protein complex and dissociation of MyD88 from the actin cytoskeleton to the cytoplasm (Fig. 4A to E). NO also reduces the interaction of MyD88 with TIRAP (Fig. 3). These effects may ultimately result in mitigated potential for the ligation-dependent recruitment of MyD88 to TLRs.

We found that S nitrosylation of MyD88 plays some roles in NO modulation of TLR signal transduction. Interestingly, eight of the nine cysteine residues of MyD88 are concentrated in the TIR domain, but the C-terminal DD contains no cysteine residue, suggesting that cysteine modification affects TIR-TIR interaction but not DD-DD interaction. Indeed, NO attenuated the interaction of MyD88 with TIRAP but not that with IRAK-1 (Fig. 3). This result is supported by the result found by Xiong et al. (52) showing that SNAP treatment did

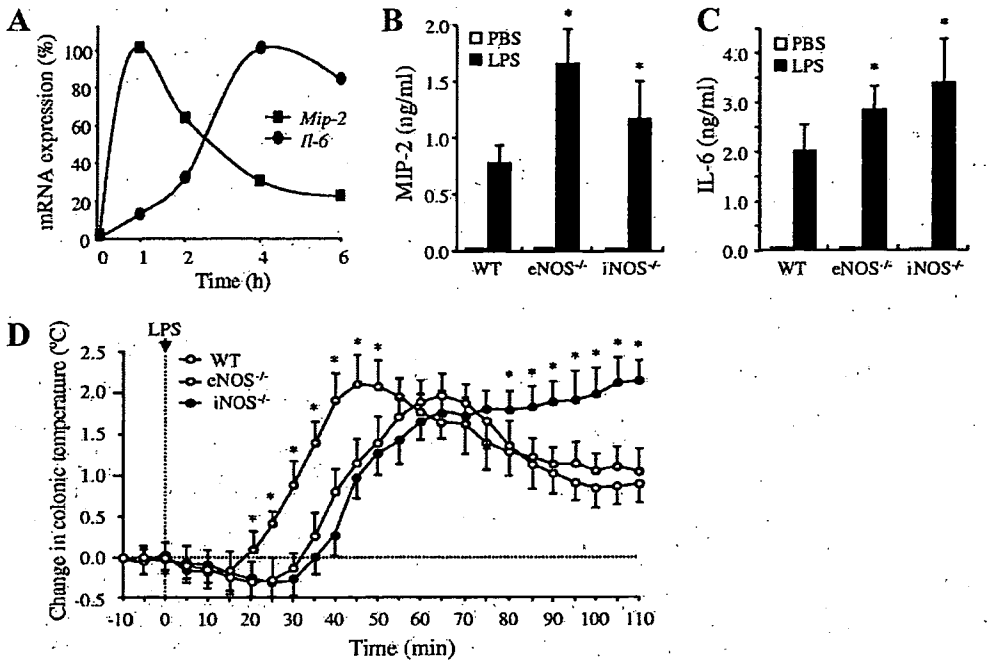

FIG. 6. Roles of eNOS and iNOS in early innate immune responses in vivo. (A) Peritoneal macrophages from wild-type mice were stimulated with 100 ng/ml LPS and 10 ng/ml gamma interferon for the indicated periods. Then, expression levels of mRNAs of *Mip-2* and *Il-6* were determined by quantitative PCR. Percent mRNA expression was calculated by taking the maximum values of mRNA levels of *Mip-2* and *Il-6* as 100%. (B, C) Wild-type (WT), eNOS$^{-/-}$, and iNOS$^{-/-}$ mice were i.p. treated with LPS. After 2 h, PBS was injected into the abdominal cavity and fluids were collected for measurement of the amounts of MIP-2 (B) and IL-6 (C) by ELISA. Each value is the mean ± SD ($n = 6$). (*, $P < 0.01$ for comparison with wild-type mice). (D) Wild-type, eNOS$^{-/-}$, and iNOS$^{-/-}$ mice were i.p. treated with LPS. The colonic temperature was monitored at 5-min intervals during a period of 10 min before and 120 min after LPS administration. Each value is the mean ± SD ($n = 6$). (*, $P < 0.01$ for comparison with wild-type mice).

not affect the interaction of MyD88 with IRAK-1 in mouse macrophages. Although S nitrosylation of the Cys216 residue of MyD88 may participate in the NO regulation of TLR signal transduction, it is likely that this modification does not have a dominant effect, because Cys216 was not essential for activation of downstream signaling (Fig. 1G). NO modification of Cys216 may yield a slight structural change in the base of the TIR domain, resulting in slightly reduced interaction with a counterpart TIR domain of TIRAP. Alternatively, NO may antagonize other reversible modifications, such as palmitoylation or disulfide bonding to a counterpart molecule, leading to transient impairment of MyD88 functioning. Also, other unknown mechanisms for MyD88 regulation may be negatively influenced by S nitrosylation.

We found that eNOS and iNOS differentially regulate LPS-induced acute-phase immune responses in vivo (Fig. 6). Although the amount of NO derived from eNOS is comparatively small, NO is steadily generated from endothelial cells as a vasodilatory gas that continually maintains an antiproliferative and antiapoptotic environment in vasculatures (16). Simultaneously, eNOS increases the amounts of cellular S-nitrosylated proteins and circulating NO donors by nitrosylating GSH and albumin (40). Such functions of NO from eNOS may systemically reduce cellular reactivity to a TLR stimulus to maintain a weak tolerance, which may lead to prevention of a rapid rise of inflammation. In contrast, NO from iNOS is generated in large quantities and exerts a strong antimicrobial action, although NO from eNOS also has an antimicrobial property (4, 29). The large amount of NO derived from iNOS is thought to disrupt cellular signaling cascades, resulting in anti-inflammatory or immunosuppressive effects. Such functions of NO from iNOS may regionally reduce cellular reactivity to TLR recognition of pathogens to initiate an inducible tolerance, which may transiently prevent promotion of excess inflammatory responses, although excess NO production ultimately results in nitrosative stress and apoptotic cell death (12, 26).

Our study proposes that TLR signal transduction involves an oxidative protein modification by NO and its redox regulation. NO may exert other effects, such as activation of cyclic-GMP-dependent signaling, on TLR signaling events, but such effects may not be dominant, at least in the acute-phase innate immune responses. Further investigations will be necessary to clarify more details about the relationship between such NO regulation and physiological or pathophysiological innate immune responses.

ACKNOWLEDGMENTS

We thank Margaret K. Offermann (Emory University School of Medicine) for providing DNA constructs of human MyD88 and TIRAP.

This work was supported by grants-in-aid for Scientific Research on Priority Areas (19041079 to T. Into) and for Young Scientists (B: 18791363 to T. Into), provided by the Ministry of Education, Culture, Sports, Science and Technology, Japan.

REFERENCES

1. **Akira, S., and K. Takeda.** 2004. Toll-like receptor signalling. Nat. Rev. Immunol. 4:499–511.

2. **Akira, S., S. Uematsu, and O. Takeuchi.** 2006. Pathogen recognition and innate immunity. Cell **124**:783–801.
3. **Blatteis, C. M., E. Sehic, and S. Li.** 2000. Pyrogen sensing and signaling: old views and new concepts. Clin. Infect. Dis. **31**:S168–177.
4. **Bogdan, C.** 2001. Nitric oxide and the immune response. Nat. Immunol. **2**:907–916.
5. **Dai, Q., and S. B. Pruett.** 2006. Ethanol suppresses LPS-induced Toll-like receptor 4 clustering, reorganization of the actin cytoskeleton, and associated TNF-α production. Alcohol Clin. Exp. Res. **30**:1436–1444.
6. **Dimmeler, S., J. Haendeler, M. Nehls, and A. M. Zeiher.** 1997. Suppression of apoptosis by nitric oxide via inhibition of interleukin-1β-converting enzyme (ICE)-like and cysteine protease protein (CPP)-32-like proteases. J. Exp. Med. **185**:601–607.
7. **Farrar, M. A., I. Alberol, and R. M. Perlmutter.** 1996. Activation of the Raf-1 kinase cascade by coumermycin-induced dimerization. Nature **383**:178–181.
8. **Forrester, M. T., M. W. Foster, and J. S. Stamler.** 2007. Assessment and application of the biotin switch technique for examining protein *S*-nitrosylation under conditions of pharmacologically induced oxidative stress. J. Biol. Chem. **282**:13977–13983.
9. **Forstermann, U., J. P. Boissel, and H. Kleinert.** 1998. Expressional control of the 'constitutive' isoforms of nitric oxide synthase (NOS I and NOS III). FASEB J. **12**:773–790.
10. **Ghosh, S., and M. Karin.** 2002. Missing pieces in the NF-κB puzzle. Cell **109**:S81–96.
11. **Häcker, H., V. Redecke, B. Blagoev, I. Kratchmarova, L. C. Hsu, G. G. Wang, M. P. Kamps, E. Raz, H. Wagner, G. Hacker, M. Mann, and M. Karin.** 2006. Specificity in Toll-like receptor signalling through distinct effector functions of TRAF3 and TRAF6. Nature **439**:204–207.
12. **Hara, M. R., N. Agrawal, S. F. Kim, M. B. Cascio, M. Fujimuro, Y. Ozeki, M. Takahashi, J. H. Cheah, S. K. Tankou, L. D. Hester, C. D. Ferris, S. D. Hayward, S. H. Snyder, and A. Sawa.** 2005. *S*-nitrosylated GAPDH initiates apoptotic cell death by nuclear translocation following Siah1 binding. Nat. Cell Biol. **7**:665–674.
13. **Hayden, M. S., A. P. West, and S. Ghosh.** 2006. NF-κB and the immune response. Oncogene **25**:6758–6780.
14. **Hess, D. T., A. Matsumoto, S. O. Kim, H. E. Marshall, and J. S. Stamler.** 2005. Protein *S*-nitrosylation: purview and parameters. Nat. Rev. Mol. Cell Biol. **6**:150–166.
15. **Hoffmann, J., J. Haendeler, A. M. Zeiher, and S. Dimmeler.** 2001. TNFα and oxLDL reduce protein *S*-nitrosylation in endothelial cells. J. Biol. Chem. **276**:41383–41387.
16. **Ignarro, L. J.** 2002. Nitric oxide as a unique signaling molecule in the vascular system: a historical overview. J. Physiol. Pharmacol. **53**:503–514.
17. **Into, T., J. Dohkan, M. Inomata, M. Nakashima, K. Shibata, and K. Matsushita.** 2007. Synthesis and characterization of a dipalmitoylated lipopeptide derived from paralogous lipoproteins of *Mycoplasma pneumoniae*. Infect. Immun. **75**:2253–2259.
18. **Into, T., Y. Kanno, J. Dohkan, M. Nakashima, M. Inomata, K. Shibata, C. J. Lowenstein, and K. Matsushita.** 2007. Pathogen recognition by Toll-like receptor 2 activates Weibel-Palade body exocytosis in human aortic endothelial cells. J. Biol. Chem. **282**:8134–8141.
19. **Into, T., and K. Shibata.** 2005. Apoptosis signal-regulating kinase 1-mediated sustained p38 mitogen-activated protein kinase activation regulates mycoplasmal lipoprotein- and staphylococcal peptidoglycan-triggered Toll-like receptor 2 signalling pathways. Cell. Microbiol. **7**:1305–1317.
20. **Iwasaki, A., and R. Medzhitov.** 2004. Toll-like receptor control of the adaptive immune responses. Nat. Immunol. **5**:987–995.
21. **Jaffrey, S. R., H. Erdjument-Bromage, C. D. Ferris, P. Tempst, and S. H. Snyder.** 2001. Protein *S*-nitrosylation: a physiological signal for neuronal nitric oxide. Nat. Cell Biol. **3**:193–197.
22. **Jaunin, F., K. Burns, J. Tschopp, T. E. Martin, and S. Fakan.** 1998. Ultrastructural distribution of the death-domain-containing MyD88 protein in HeLa cells. Exp. Cell Res. **243**:67–75.
23. **Kagan, J. C., and R. Medzhitov.** 2006. Phosphoinositide-mediated adaptor recruitment controls Toll-like receptor signaling. Cell **125**:943–955.
24. **Karin, M., and F. R. Greten.** 2005. NF-κB: linking inflammation and immunity to cancer development and progression. Nat. Rev. Immunol. **5**:749–759.
25. **Kelleher, Z. T., A. Matsumoto, J. S. Stamler, and H. E. Marshall.** 2007. NOS2 regulation of NF-κB by *S*-nitrosylation of p65. J. Biol. Chem. **282**: 30667–30672.
26. **Kim, K. M., P. K. Kim, Y. G. Kwon, S. K. Bai, W. D. Nam, and Y. M. Kim.** 2002. Regulation of apoptosis by nitrosative stress. J. Biochem. Mol. Biol. **35**:127–133.
27. **Laroux, F. S., X. Romero, L. Wetzler, P. Engel, and C. Terhorst.** 2005. MyD88 controls phagocyte NADPH oxidase function and killing of gram-negative bacteria. J. Immunol. **175**:5596–5600.
28. **Lawrence, T., M. Bebien, G. Y. Liu, V. Nizet, and M. Karin.** 2005. IKKα limits macrophage NF-κB activation and contributes to the resolution of inflammation. Nature **434**:1138–1143.
29. **MacMicking, J., Q. W. Xie, and C. Nathan.** 1997. Nitric oxide and macrophage function. Annu. Rev. Immunol. **15**:323–350.
30. **Mannick, J. B., A. Hausladen, L. Liu, D. T. Hess, M. Zeng, Q. X. Miao, L. S. Kane, A. J. Gow, and J. S. Stamler.** 1999. Fas-induced caspase denitrosylation. Science **284**:651–654.
31. **Mannick, J. B., C. Schonhoff, N. Papeta, P. Ghafourifar, M. Szibor, K. Fang, and B. Gaston.** 2001. *S*-Nitrosylation of mitochondrial caspases. J. Cell Biol. **154**:1111–1116.
32. **Marshall, H. E., D. T. Hess, and J. S. Stamler.** 2004. *S*-nitrosylation: physiological regulation of NF-κB. Proc. Natl. Acad. Sci. USA **101**:8841–8842.
33. **Marshall, H. E., and J. S. Stamler.** 2001. Inhibition of NF-κB by *S*-nitrosylation. Biochemistry **40**:1688–1693.
34. **Matsuzawa, A., K. Saegusa, T. Noguchi, C. Sadamitsu, H. Nishitoh, S. Nagai, S. Koyasu, K. Matsumoto, K. Takeda, and H. Ichijo.** 2005. ROS-dependent activation of the TRAF6-ASK1-p38 pathway is selectively required for TLR4-mediated innate immunity. Nat. Immunol. **6**:587–592.
35. **Medzhitov, R., P. Preston-Hurlburt, and C. A. Janeway, Jr.** 1997. A human homologue of the Drosophila Toll protein signals activation of adaptive immunity. Nature **388**:394–397.
36. **Medzhitov, R., P. Preston-Hurlburt, E. Kopp, A. Stadlen, C. Chen, S. Ghosh, and C. A. Janeway, Jr.** 1998. MyD88 is an adaptor protein in the hToll/IL-1 receptor family signaling pathways. Mol. Cell **2**:253–258.
37. **Miggin, S. M., E. Palsson-McDermott, A. Dunne, C. Jefferies, E. Pinteaux, K. Banahan, C. Murphy, P. Moynagh, M. Yamamoto, S. Akira, N. Rothwell, D. Golenbock, K. A. Fitzgerald, and L. A. O'Neill.** 2007. NF-κB activation by the Toll-IL-1 receptor domain protein MyD88 adapter-like is regulated by caspase-1. Proc. Natl. Acad. Sci. USA **104**:3372–3377.
38. **Park, H. S., J. W. Yu, J. H. Cho, M. S. Kim, S. H. Huh, K. Ryoo, and E. J. Choi.** 2004. Inhibition of apoptosis signal-regulating kinase 1 by nitric oxide through a thiol redox mechanism. J. Biol. Chem. **279**:7584–7590.
39. **Reynaert, N. L., K. Ckless, S. H. Korn, N. Vos, A. S. Guala, E. F. Wouters, A. van der Vliet, and Y. M. Janssen-Heininger.** 2004. Nitric oxide represses inhibitory κB kinase through *S*-nitrosylation. Proc. Natl. Acad. Sci. USA **101**:8945–8950.
40. **Richardson, G., and N. Benjamin.** 2002. Potential therapeutic uses for *S*-nitrosothiols. Clin. Sci. (London) **102**:99–105.
41. **Rubin, D. B., G. Reznik, E. A. Weiss, and P. R. Young.** 2000. Non-protein thiols flux to *S*-nitrosothiols in endothelial cells: an LPS redox signal. Shock **14**:200–207.
42. **Stamler, J. S., S. Lamas, and F. C. Fang.** 2001. Nitrosylation. The prototypic redox-based signaling mechanism. Cell **106**:675–683.
43. **Stamler, J. S., D. I. Simon, J. A. Osborne, M. E. Mullins, O. Jaraki, T. Michel, D. J. Singel, and J. Loscalzo.** 1992. *S*-nitrosylation of proteins with nitric oxide: synthesis and characterization of biologically active compounds. Proc. Natl. Acad. Sci. USA **89**:444–448.
44. **Steiner, A. A., S. Chakravarty, A. Y. Rudaya, M. Herkenham, and A. A. Romanovsky.** 2006. Bacterial lipopolysaccharide fever is initiated via Toll-like receptor 4 on hematopoietic cells. Blood **107**:4000–4002.
45. **Steiner, A. A., A. Y. Rudaya, A. I. Ivanov, and A. A. Romanovsky.** 2004. Febrigenic signaling to the brain does not involve nitric oxide. Br. J. Pharmacol. **141**:1204–1213.
46. **Thoma-Uszynski, S., S. Stenger, O. Takeuchi, M. T. Ochoa, M. Engele, P. A. Sieling, P. F. Barnes, M. Rollinghoff, P. L. Bolcskei, M. Wagner, S. Akira, M. V. Norgard, J. T. Belisle, P. J. Godowski, B. R. Bloom, and R. L. Modlin.** 2001. Induction of direct antimicrobial activity through mammalian Toll-like receptors. Science **291**:1544–1547.
47. **Uematsu, S., M. Matsumoto, K. Takeda, and S. Akira.** 2002. Lipopolysaccharide-dependent prostaglandin E(2) production is regulated by the glutathione-dependent prostaglandin E(2) synthase gene induced by the Toll-like receptor 4/MyD88/NF-IL6 pathway. J. Immunol. **168**:5811–5816.
48. **Vulcano, M., S. Dusi, D. Lissandrini, R. Badolato, P. Mazzi, E. Riboldi, E. Borroni, A. Calleri, M. Donini, A. Plebani, L. Notarangelo, T. Musso, and S. Sozzani.** 2004. Toll receptor-mediated regulation of NADPH oxidase in human dendritic cells. J. Immunol. **173**:5749–5756.
49. **Wang, W., A. Mitra, B. Poole, S. Falk, M. S. Lucia, S. Tayal, and R. Schrier.** 2004. Endothelial nitric oxide synthase-deficient mice exhibit increased susceptibility to endotoxin-induced acute renal failure. Am. J. Physiol. Renal Physiol. **287**:F1044–F1048.
50. **West, M. B., B. G. Hill, Y. T. Xuan, and A. Bhatnagar.** 2006. Protein glutathiolation by nitric oxide: an intracellular mechanism regulating redox protein modification. FASEB J. **20**:1715–1717.
51. **Woronicz, J. D., X. Gao, Z. Cao, M. Rothe, and D. V. Goeddel.** 1997. IκB kinase-β: NF-κB activation and complex formation with IκB kinase-α and NIK. Science **278**:866–869.
52. **Xiong, H., C. Zhu, F. Li, R. Hegazi, K. He, M. Babyatsky, A. J. Bauer, and S. E. Plevy.** 2004. Inhibition of interleukin-12 p40 transcription and NF-κB activation by nitric oxide in murine macrophages and dendritic cells. J. Biol. Chem. **279**:10776–10783.
53. **Yamawaki, H., J. Haendeler, and B. C. Berk.** 2003. Thioredoxin: a key regulator of cardiovascular homeostasis. Circ. Res. **93**:1029–1033.

Cardiovascular Research (2008) 77, 221–230
doi:10.1093/cvr/cvm049

Nitric oxide regulates vascular calcification by interfering with TGF-β signalling

Yosuke Kanno[1,2*], Takeshi Into[1], Charles J. Lowenstein[3], and Kenji Matsushita[1*]

[1]*Department of Oral Disease Research, National Center for Geriatrics and Gerontology, 36-3 Gengo, Morioka-cho, Obu, Aichi 474-8511, Japan;* [2]*Department of Clinical Pathological Biochemistry, Faculty of Pharmaceutical Science, D.W.C.L.A., Kyo-tanabe, Kyoto 610-0395, Japan; and* [3]*The Johns Hopkins University School of Medicine, Baltimore, MD 21205, USA*

Received 27 March 2007; revised 3 October 2007; accepted 21 October 2007; online publish-ahead-of-print 25 October 2007

Time for primary review: 19 days

KEYWORDS
Atherosclerosis;
Vascular calcification;
Vascular ageing;
Diabetes mellitus

Aims Vascular calcification often occurs with advancing age, atherosclerosis, and metabolic disorders such as diabetes mellitus and end-stage renal disease. Vascular calcification is associated with cardiovascular events and increased mortality. Nitric oxide (NO) is crucial for maintaining vascular function, but little is known about how NO affects vascular calcification. The aim of this study was to examine the effect of NO on vascular calcification.

Methods and results In this study, we examined the inhibitory effects of NO on calcification of murine vascular smooth muscle cells (VSMCs) *in vitro*. We measured calcium concentration, alizarin red staining, and alkaline phosphatase activity to examine the effect of NO on calcification of VSMCs and differentiation of VSMCs into osteoblastic cells. We also determined gene expression and levels of phosphorylation of Smad2/3 by RT–PCR and western blotting. NO inhibited calcification of VSMCs and differentiation of VSMCs into osteoblastic cells. An inhibitor of cyclic guanosine monophosphate (cGMP)-dependent protein kinase restored the inhibition by NO of osteoblastic differentiation and calcification of VSMCs. NO inhibited transforming growth factor-β (TGF-β)-induced phosphorylation of Smad2/3 and expression of TGF-β-induced genes such as plasminogen activator inhibitor-1. In addition, NO inhibited expression of the TGF-β receptor ALK5.

Conclusion Our data show that NO prevents differentiation of VSMCs into osteoblastic cells by inhibiting TGF-β signalling through a cGMP-dependent pathway. Our findings suggest that NO may play a beneficial role in atherogenesis in part by limiting vascular calcification.

Introduction

Vascular calcification occurs in many diseases, including atherosclerosis, diabetes, and uremia.[1–3] Deposition of calcification in arteries diminishes arterial wall elasticity, obstructs blood flow, and can lead to heart attacks and stroke.[4] The presence of calcium deposits in the vessel wall is indicative of advanced atherosclerosis, and the extent of coronary calcification adds independent prognostic significance to conventional risk factors for coronary artery disease. Vascular calcification is a major independent predictor of cardiovascular morbidity and mortality.[5]

Vascular calcification has been considered to be an organized, regulated process similar to mineralization in bone tissue.[6,7] Specific bone-associated proteins such as matrix Gla protein are constitutively expressed at low levels in the healthy vessel, and their expression increases during vascular calcification.[8,9] Moreover, the expression of a number of bone-associated proteins such as osteopontin normally absent in the vessel wall is also increased in the calcified vessel wall.[9]

Vascular smooth muscle cells (VSMCs) play a major role in vascular calcification.[10] VSMCs contribute to the development of an atherosclerotic lesion by migration, proliferation, and secretion of matrix components.[11,12] VSMCs also express many of the calcification-regulating proteins commonly found in bone.[8–9,13] These proteins have calcium and apatite binding properties, and accumulate in areas of vascular calcification. Among them, transforming growth factor-β (TGF-β) is a key factor in vascular calcification. TGF-β is present in calcified aortic valves,[14] and regulates vascular calcification and osteoblastic differentiation of VSMCs.[6,15]

Nitric oxide (NO) is a messenger molecule produced by the NO synthase (NOS) isoforms neuronal NOS (nNOS, or NOS1), inducible NOS (iNOS, or NOS2), and endothelial NOS (eNOS, or NOS3).[16,17] All three NOS isoforms can be found in the vasculature – NOS1 in nerve fibbers in the adventitia,

* Corresponding author. Tel: +81 0774 65 8629; fax: +81 0774 65 8479.
E-mail address: ykanno@dwc.doshisha.ac.jp (Y.K.). Tel: +81 562 46 2311 (ext. 5401); fax:+81 562 46 8479. *E-mail address*: kmatsu30@nils.go.jp (K.M.)

NOS2 in VSMCs and in infiltrating macrophages during vascular inflammation, and NOS3 in endothelial cells – and NO has a variety of effects upon vascular cells. NO produced in the endothelium by eNOS activates smooth muscle cell relaxation and vasodilation by binding to soluble guanylate cyclase, resulting in cyclic guanosine monophosphate (cGMP) production and the activation of signal transduction pathways. NO also inhibits smooth muscle cell migration and proliferation.[18,19] NO may also affect vascular calcification. However, the effect of NO on vascular calcification is not understood.

Although TGF-β induces vascular calcification, the regulatory mechanism of vascular calcification is not well clarified. We hypothesized that NO inhibits vascular calcification by regulating TGF-β signalling. Here we show that NO regulates vascular calcification in part by interfering with TGF-β signalling.

Methods

All experiments were performed in accordance with the Guide for the Care and Use of Laboratory Animals published by the US National Institutes of Health.

Reagents

Recombinant human TGF-β_1 and 8-bromo-cGMP were from Calbiochem (Daemsradt USA). The NO donor DETA-NONOate was from Cayman Chemical Co. (Ann Arbor, MI, USA). The NOS inhibitor aminoguanidine hemisulphate (AG) was purchased from Sigma-Aldrich (St Louis, MO, USA). The guanylate cyclase inhibitor ODQ was from Wako Pure Chemical (Osaka, Japan). The protein kinase G (PKG) inhibitor KT5823 was from Sigma-Aldrich.

Cell culture and analysis of vascular smooth muscle cell calcification

VSMCs were obtained from the thoracic aorta of C57BL/6J mice.[20] Induction of calcification of VSMCs was performed by a procedure of Tintut *et al.*[21] with minor modifications. VSMCs were grown in Dulbecco's modified Eagle's medium (Sigma-Aldrich) containing 10% heat-inactivated foetal bovine serum and supplemented with 1 mM sodium pyruvate, 100 units/ml penicillin, and 100 units/mL streptomycin. After 4 days, the media was replaced with calcification media (media supplemented with 5 mM β-glycerophosphate and 4 mM $CaCl_2$) to permit maximal mineralization. The calcification media were changed every 3–4 days. To examine the effect of NO on VSMC calcification, VSMCs were grown in calcification media with DETA-NONOate for 14 days. To become 10 μM, we added DETA NONOate at intervals of 20 h.

To determine the degree of mineralization, calcium concentration in the cells was measured by Calcium Assay Kit (BioAssay Systems). After 14 days in culture, cells were then washed, and proteins in cells were extracted with a lysis buffer (10 mM Tris–HCl, pH 7.5, 0.1% Triton X-100). A phenolsulphonephthalein dye in the kit forms a very stable blue coloured complex specifically with free calcium. The intensity of the colour, measured at 612 nm, is directly proportional to the calcium concentration in the sample.

Alizarin red staining

Calcified VSMCs were stained with alizarin red S (Kanto Chemical, Japan). After washing, cultures were fixed with 4% paraformaldehyde in PBS for 15 min, and then stained with 2% alizarin red S in H_2O for 30 min at room temperature. After staining, cultures were washed three times.

Cell viability assays

Cell viability was assessed as a function of NADH content using a TetraColor ONE [5 mM (2-(2-methoxy-4-nytrophenyl)-3-(4-nitrophenyl)-5-(2,4-disulphophenyl)-2*H*-tetrazolium, monosodium salt); 0.2 mM 1-methoxy-5-metylphenazinium methylsulphate; and 150 mM NaCl]-based assay according to the manufacturer's instructions (Seikagaku Inc., Nihonbashi, Tokyo, Japan). VSMCs were grown in calcification media with DETA-NONOate for 14 days. After 14 days, cell viability was evaluated using TetraColor ONE (Seikagaku Corp.). Finally, 10 μL of TetraColor ONE solution was added to each well, and the cells were incubated for 1.5 h. A well for the negative control was prepared as described above without cells. The absorbance of each well was then determined at a wavelength of 450 nm.

Measurement of alkaline phosphatase activity

VSMCs were seeded at a density of 4×10^5 cells/well on six-well plates. After 14 days in culture, cells were then washed, and proteins in cells were extracted with a lysis buffer (10 mM Tris–HCl, pH 7.5, 0.1% Triton X-100). Alkaline phosphatase (ALP) activity was determined using *p*-nitro phenyl phosphate (Sigma-Aldrich) as a substrate. Protein concentration of extracts was determined by BCA protein assay kit (Pierce) using bovine serum albumin as a standard.

Inducible nitric oxide synthase and endothelial nitric oxide synthase overexpressing vascular smooth muscle cells

VSMCs were transfected with iNOS (mouse) and eNOS (bovine) plasmid (pcDNA 3.1/His 'A' vector) by using Lipofectamine 2000. From the second day after the transfection, iNOS or eNOS or empty vector-transfected cells were selected with 200 μg/mL G418 for 4 weeks. These VSMCs were cultured as described above.

Reverse transcription-polymerase chain reaction

Total RNA was isolated from VSMCs using Isogen (Nippon Gene, Japan) and was reverse-transcribed using MMLV reverse transcriptase (GIBCO BRL). The transcripts were amplified by PCR using Ex *Taq* (TaKaRa, Japan). The following primers were synthesized: PAI-1 sense, AAAGGTATGATCAATGACTTACTGG; PAI-1 antisense, TCAAAGGGTGCAGCGATGAACATGC; ALK1 sense, TGACTTTCTGCAGAGGCAGA; ALK1 antisense, CGACTCAAAGCAGTCTGTGC; ALK5 sense, ATCCATCACTAGATCGCCCT; ALK5 antisense, CGATGGATCAGAAGGTACAAGA; type I collagen sense, ATCCCCATGACTGTCTATAG; type I collagen antisense, CAAATAAGTGACCATCGCCA; osteocalcin (OC) sense, TGCGCTCTGTCTCTCTGACC; OC antisense, CTGTGACATCCATACTTGCAGG; matrix Gla protein 2 (MGP2) sense, ACCACGTCCCAGCTTCTAGC; and MGP2 antisense, GCTCTGCGATGGAGAGGTACTG; PCR amplification of cDNA for 35 cycles was at 94°C denaturation (60 s), 60°C annealing (60 s), and 72°C extension (60 s). Following PCR amplifications, the amplified cDNAs were further extended by additional incubation at 72°C for 10 min. An equal amount of each reaction was fractionated on 1% agarose gel in 1 × TAE buffer, and then the agarose gel was soaked in 1 × TAE buffer containing ethidium bromide for 15 min by gentle agitation. The amplified cDNA fragments in the agarose gel were then visualized on a UV transilluminator and photographed.

Western blot analysis for Smad2/3

VSMCs grown in a six-well plate were washed twice with ice-cold PBS; lysed with 62.5 mM Tris–HCl (pH 6.8) containing 2% SDS, 10% glycerol, and 50 mM DTT (an SDS sample buffer) in the presence of inhibitor cocktails of proteases (Sigma-Aldrich); and boiled for 10 min. The lysates were centrifuged at 14 000 rpm for 10 min, and the resulting supernatants containing cytosolic and membrane proteins were collected. Proteins in the supernatant were separated

by electrophoresis on 10% SDS-polyacrylamide gels and transferred to a nitrocellulose membrane. The membrane was incubated at 4°C overnight with polyclonal antibody to Smad2/3 or antibody to phospho-Smad2/3 and then with peroxidase-conjugated antibody to rabbit IgG. Immunoreactive proteins were detected using ECL detection reagents (Amersham Pharmacia Biotech).

Statistical analysis

All data are expressed as mean ± SEM. The significance of the effect of each treatment ($P < 0.05$) was determined by analysis of variance (ANOVA) followed by the Student Newman-Keuls test.

Results

Nitric oxide inhibits vascular smooth muscle cell calcification

To explore the effect of NO on vascular calcification, we incubated VSMCs from murine aorta in DMEM media supplemented with 5 mM β-glycerophosphate and 4 mM $CaCl_2$ (calcification media) in the presence or absence of DETA-NONOate for 14 days, and then the amount of calcification in cells were measured by alizarin red staining. Calcification media induced mineralization of VSMCs. However, the NO donor inhibits VSMC calcification (*Figure 1A* and *B*). The NO donor did not affect on the cell viability (*Figure 1C*).

To explore the role of NO in the regulation of vascular calcification, we first measured NOS mRNA expression in VSMCs and calcified VSMCs by RT–PCR. VSMCs expressed mRNAs of eNOS and iNOS, and the expression levels were increased in calcified VSMCs (*Figure 1D*). Calcified VSMCs also expressed nNOS mRNA. We next treated calcifying VSMCs with an NO inhibitor AG for 14 days and measured calcification. AG increased VSMC calcification (*Figure 1E*). Moreover, we examined the effect of iNOS and eNOS on VSMCs calcification by transfection of iNOS and eNOS plasmid (*Figure 1F*). iNOS and eNOS overexpression inhibited VSMC calcification (*Figure 1G*). These data suggest NO regulates vascular calcification.

Nitric oxide inhibits osteoblastic differentiation of vascular smooth muscle cells

We next examined the effect of NO on osteoblastic differentiation of VSMCs. ALP, one of the phenotypic markers of osteoblasts, is thought to be essential to bone mineralization.[22] Increased ALP activity was observed in calcified matrix vesicles of smooth muscle cells. Therefore, we examined the effect of NO on ALP activity in calcifying VSMCs. ALP activity was strongly detected in calcifying VSMCs. The NO donor inhibits ALP activity in calcifying VSMCs (*Figure 2A*). We also showed that the NO donor inhibits expression of other osteoblastic marker, type I collagen, OC, and MGP2 (*Figure 2B*). We next treated calcifying VSMCs with an NO inhibitor AG for 14 days and measured ALP activity. AG increased ALP activity of VSMC (*Figure 2C*). Moreover, we examined the effect of iNOS and eNOS on osteoblastic differentiation by transfection of iNOS and eNOS plasmid (*Figure 1F*). iNOS and eNOS overexpression inhibited osteoblastic differentiation of VSMCs (*Figure 2D*). These data suggest NO regulates osteoblastic differentiation of VSMCs.

Nitric oxide/cGMP/protein kinase G signalling pathway mediates vascular smooth muscle cell calcification

To determine whether or not NO inhibits vascular calcification through a cGMP pathway, we examined the effect of the guanylate cyclase inhibitor ODQ and the PKG inhibitor KT5823 on VSMCs calcification treated with NO. ODQ blocked the inhibitory effect of NO on VSMC calcification (*Figure 3A*). KT5823 also blocked the inhibitory effect of NO on VSMC calcification (*Figure 3B*). Furthermore, ODQ and KT5823 reversed the inhibitory effect of NO on osteoblastic differentiation (*Figure 3C* and *D*). ODQ and KT5823 increased osteoblastic differentiation in the absence of NO donor. However, ODQ and KT5823 did not increase VSMC calcification in the absence of NO donor. Then, we examined the effects of a cGMP analogue 8-bromo-cGMP on vascular calcification and osteoblastic differentiation of VSMC. Treatment with 8-bromo-cGMP inhibited VSMC calcification (*Figure 3E*). The cGMP analogue also inhibited ALP activity in calcifying VSMCs (*Figure 3F*).

Nitric oxide regulates transforming growth factor-β signalling in vascular smooth muscle cells

TGF-β regulates vascular calcification and osteoblastic differentiation of VSMCs.[6,15] Therefore, we explored the effect of NO on TGF-β signalling in VSMCs. We first examined the expression of TGF-β mRNA in calcified VSMCs by RT–PCR. Increased expression of TGF-β was observed in calcified VSMCs (*Figure 4A*). A neutralizing antibody to TGF-β inhibited VSMC calcification and osteoblastic differentiation (*Figure 4B–D*). We also examined the effect of NO on TGF-β-induced osteoblastic differentiation of VSMCs. The NO donor markedly reduced TGF-β-induced ALP activity in VSMCs (*Figure 4E*). On the other hand, TGF-β did not induce VSMC calcification in the absence of calcification media.

We next investigated whether NO affects TGF-β signalling in calcifying VSMCs. TGF-β activates a heteromeric complex of type I and type II transmembrane serine/threonine kinase receptors ALK-1 and ALK-5.[23] ALK5 activation induces phosphorylation of Smad2/3.[24] Therefore, we examined the effect of NO on Smad2/3 phosphorylation in calcifying VSMCs. The NO donor blocked TGF-β-induced phosphorylation of Smad2/3 (*Figure 5*). We also examined the effect of NO on TGF-β gene expression and its production. However, NO did not affect mRNA levels of TGF-β and TGF-β protein from calcified VSMCs (see Supplementary material online, Data 1 and 2), indicating that NO does not decrease phosphorylation of Smad2/3 by inhibiting TGF-β expression. We also investigated the effect of NO on ALK1 and ALK5 mRNA levels in calcifying VSMCs. NO markedly reduced ALK5 mRNA levels. However, NO did not reduce ALK1 mRNA (*Figure 6A*). We also investigated the effect of NO on the plasminogen activator inhibitor-1 (PAI-1) gene expression by RT–PCR, because ALK5 activates PAI-1 gene expression. NO markedly reduced mRNA expression of PAI-1 (*Figure 6B*). Moreover, we investigated the effect of KT5823 on the ALK5 and the PAI-1 gene expression treated with NO. KT5823 reversed the inhibitory effect of NO on the ALK5 and the PAI-1 gene expression (*Figure 6C*). These results suggest that NO inhibits VSMC calcification and

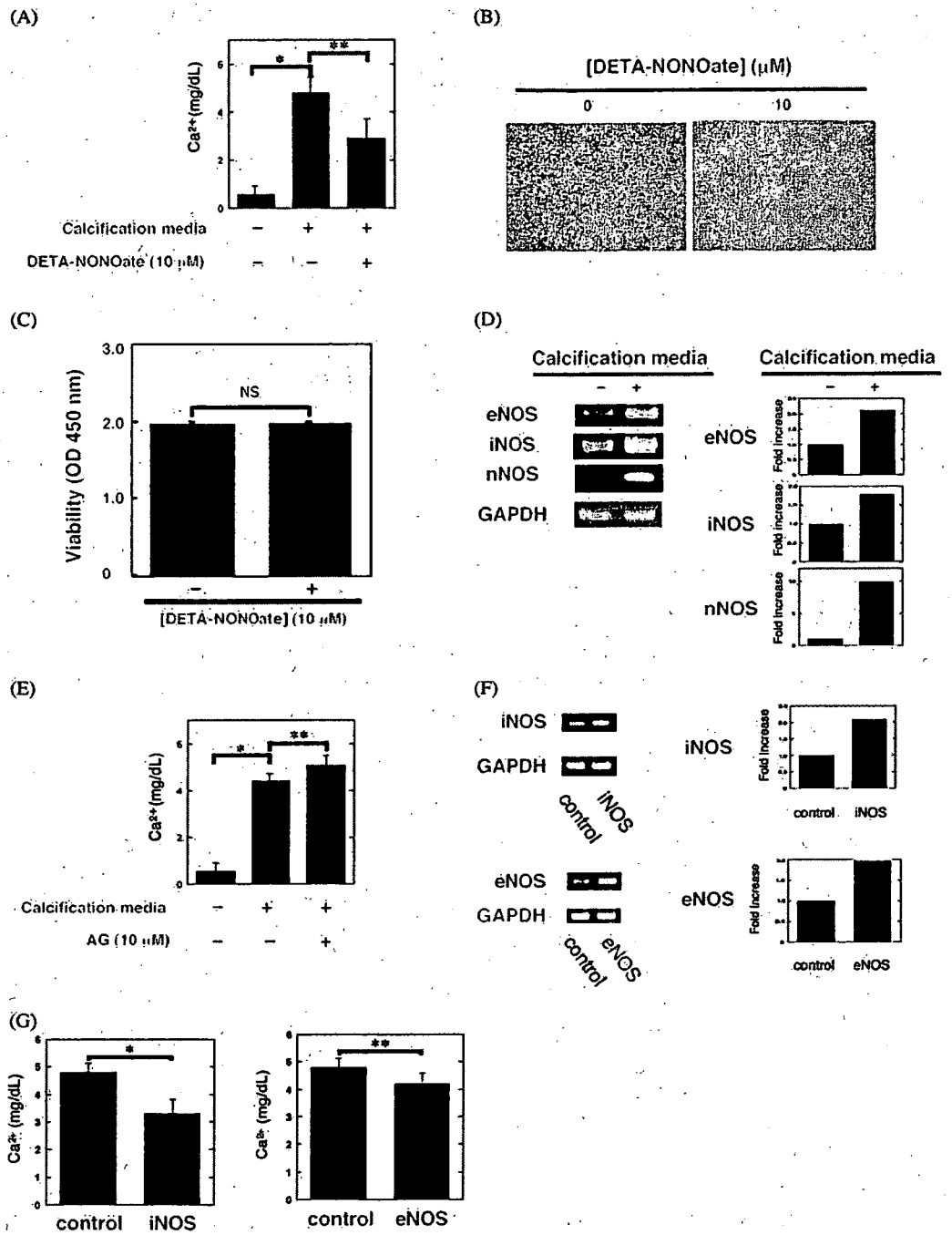

Figure 1 Nitric oxide (NO) inhibits vascular smooth muscle cell (VSMC) calcification. (*A*) VSMCs were grown with calcification media for 14 days in the presence or absence of 10 μM DETA-NONOate. Then, calcium concentration in the cells was measured as described in Methods section ($n = 5$–$6 \pm$ SEM, $^{*}P < 0.01$, $^{**}P < 0.05$). (*B*) Photomicrographs of Alizarin red staining of calcifying VSMCs treated with or without DETA-NONOate. (*C*) Effect of NO on viability of VSMCs. VSMCs were grown in calcification media with 10 μM DETA-NONOate for 14 days. Then the cell viability was assessed as a function of NADH content using a TetraColor ONE ($n = 3 \pm$ SEM). (*D*) Calcified VSMCs expressed eNOS, iNOS and nNOS. NOS expression in calcified VSMCs was measured by RT-PCR. Similar results were obtained with three additional and different samples. (*E*) NOS inhibitor increases VSMC calcification. VSMCs were grown in calcification media with an NOS inhibitor aminoguanidine hemisulphate (AG) for 14 days. Then, calcium concentration in the cells was measured as described in Methods section ($n = 5$–$6 \pm$ SEM, $^{*}P < 0.01$, $^{**}P < 0.05$). (*F*) Transfection of iNOS and eNOS plasmid significantly increased iNOS and eNOS expression, measured by RT-PCR. (*G*) NOS overexpression inhibits calcification of VSMCs. VSMCs were transfected with iNOS and eNOS plasmid. Then, VSMCs were grown with calcification media for 14 days, and calcium concentration in the cells was measured as described in Methods section ($n = 5$–$6 \pm$ SEM, $^{*}P < 0.01$, $^{**}P < 0.05$).

osteoblastic differentiation of VSMCs by regulating TGF-β signalling.

Discussion

The major finding of this study is that NO inhibits vascular calcification by interfering with TGF-β signalling.

Nitric oxide inhibits vascular calcification

We found that NO inhibited VSMC calcification and osteoblastic differentiation of VSMCs. NO inhibited an increase of ALP activity and other osteoblastic marker in calcifying VSMCs. ALP is an enzyme that has been shown to be important for matrix mineralization.[22] Osteoblasts increase ALP

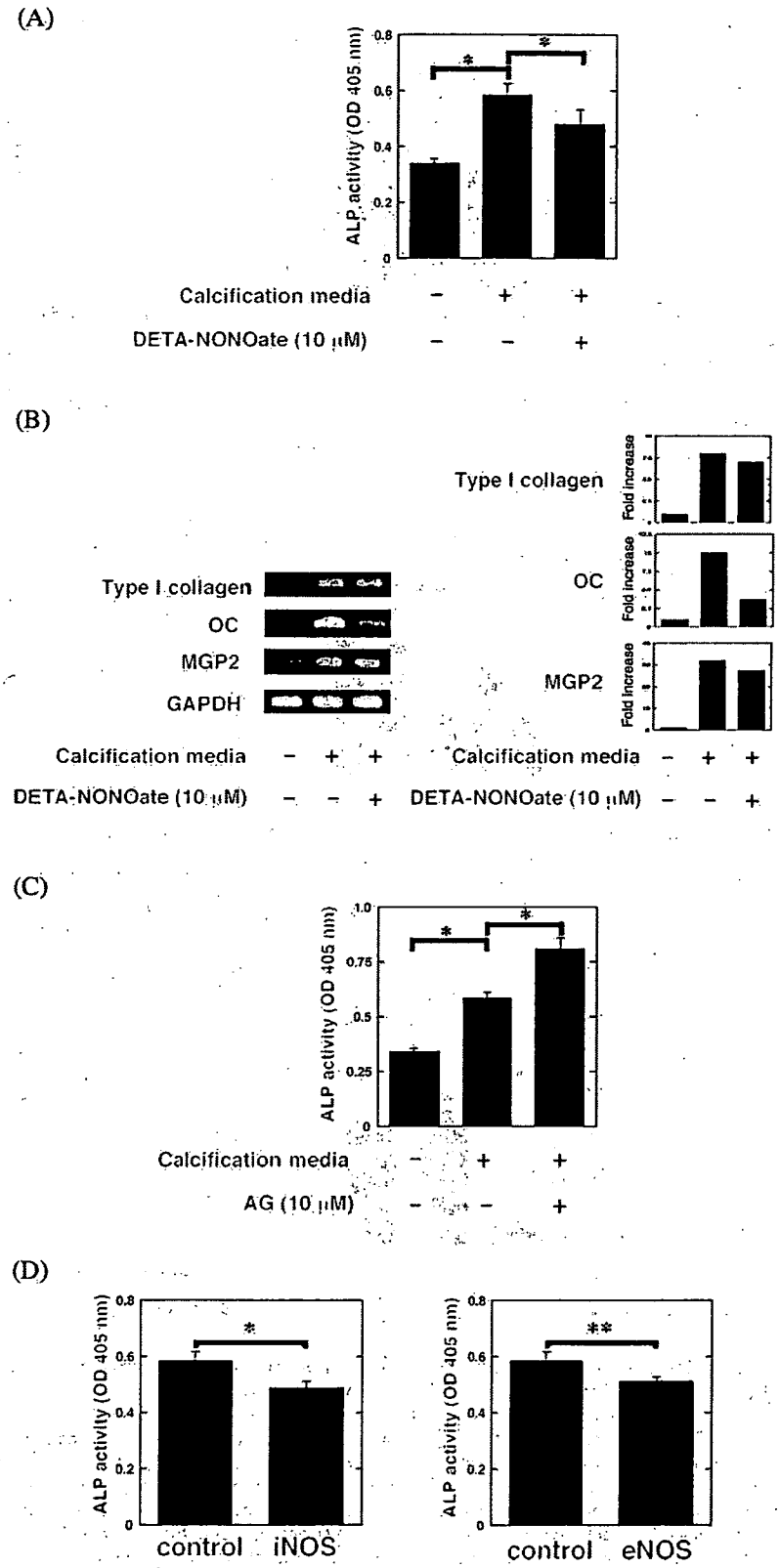

Figure 2 Nitric oxide (NO) inhibits osteoblastic differentiation of vascular smooth muscle cells (VSMCs). (*A*) NO inhibits increasing ALP activity in calcifying VSMCs. VSMCs were grown in calcification media with 10 μM DETA-NONOate for 14 days, and ALP activity at OD 405 nm was measured ($n = 6 \pm$ SEM, $^*P < 0.01$.). (*B*) NO inhibits expression of osteoblastic marker in calcifying VSMCs. VSMCs were grown in calcification media with 10 μM DETA-NONOate for 14 days, and expression of type I collagen, osteocalcin (OC) and matrix Gla protein 2 (MGP2) in calcified VSMCs was measured by RT–PCR. Similar results were obtained with three additional and different samples. (*C*) NOS inhibitor increases VSMC calcification. VSMCs were grown in calcification media with an NOS inhibitor aminoguanidine hemisulphate (AG) for 14 days, and ALP activity at OD 405 nm was measured ($n = 5$–$6 \pm$ SEM, $^*P < 0.01$, $^{**}P < 0.05$). (*D*) NOS overexpression inhibits osteoblastic differentiation of VSMCs. VSMCs were transfected with iNOS and eNOS plasmid. VSMCs were grown in calcification media for 14 days, and ALP activity at OD 405 nm was measured ($n = 6 \pm$ SEM, $^*P < 0.01$, $^{**}P < 0.05$).

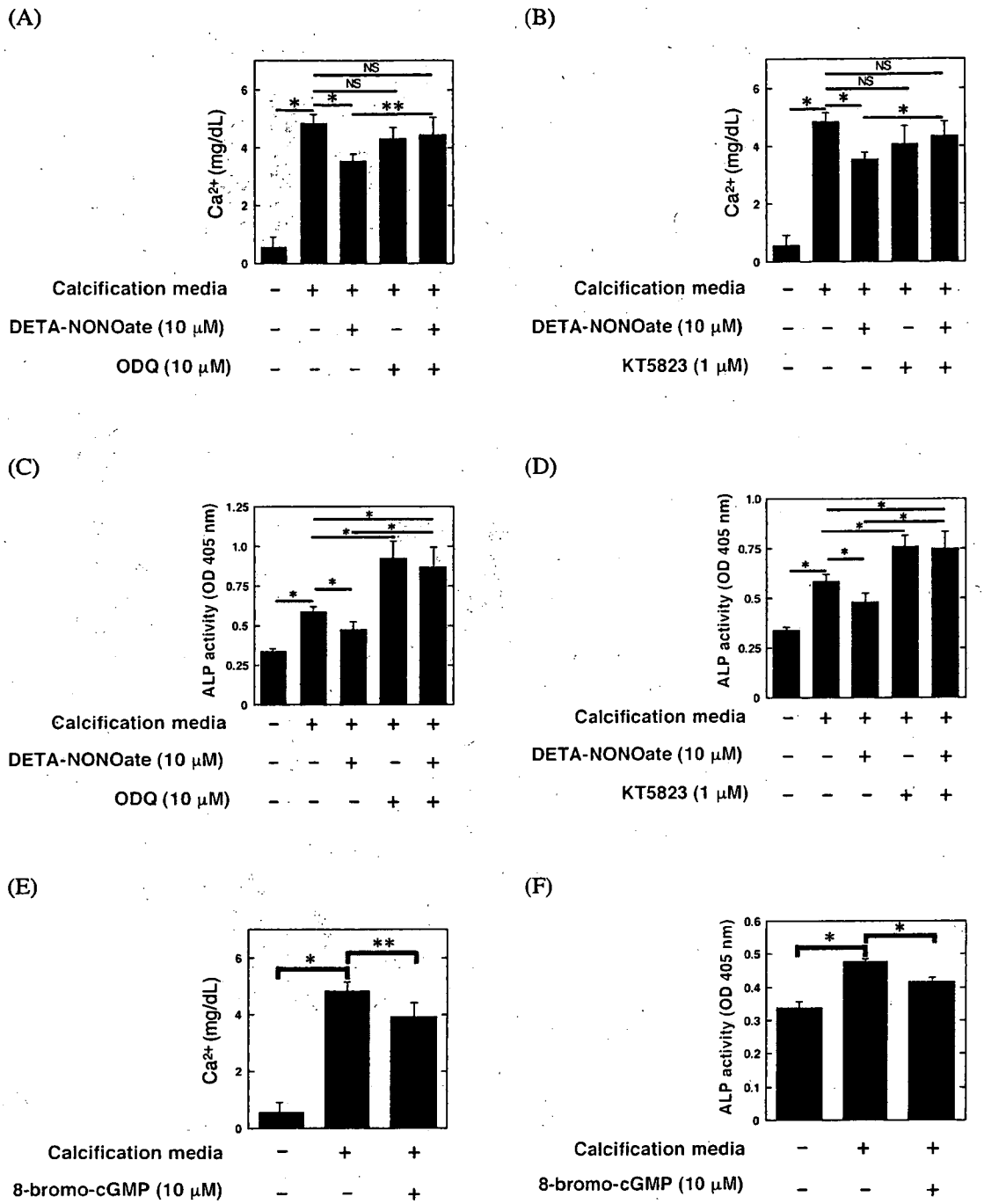

Figure 3 Nitric oxide (NO)-cGMP signalling pathway mediates vascular smooth muscle cell (VSMC) calcification. (*A*) Guanylate cyclase inhibitor ODQ blocks NO inhibition of VSMC calcification. VSMCs were grown in calcification media with 10 μM DETA-NONOate for 14 days in the presence or absence of ODQ. Then, calcium concentration in the cells was measured as described in Methods section ($n = 4$–$6 \pm$ SEM, $^*P < 0.01$, $^{**}P < 0.05$). (*B*) The PKG inhibitor KT5823 blocks NO inhibition of VSMC calcification. VSMCs were grown in calcification media with DETA-NONOate for 14 days in the presence or absence of KT5823. Mineralization was measured as above ($n = 4$–$6 \pm$ SEM, $^*P < 0.01$). (*C*) ODQ blocks NO inhibition of VSMC osteoblastic differentiation. VSMCs were grown in calcification media with 10 μM DETA-NONOate for 14 days in the presence or absence of ODQ, and ALP activity at OD 405 nm was measured ($n = 6 \pm$ SEM, $^*P < 0.01$). (*D*) KT5823 blocks NO inhibition of VSMC osteoblastic differentiation. VSMCs were grown in calcification media with DETA-NONOate for 14 days in the presence or absence of KT5823, and ALP activity at OD 405 nm was measured ($n = 6 \pm$ SEM, $^*P < 0.01$). (*E*) An analogue of cGMP, 8-bromo-cGMP, inhibits VSMC calcification. VSMCs were grown in calcification media with or without 8-bromo-cGMP for 14 days. Then, calcium concentration in the cells was measured as described in Methods section ($n = 3$–$6 \pm$ SEM, $^*P < 0.01$, $^{**}P < 0.05$). (*F*) 8-bromo-cGMP inhibits VSMC calcification. VSMCs were grown in calcification media with or without 8-bromo-cGMP for 14 days, and ALP activity at OD 405 nm was measured ($n = 3$–$6 \pm$ SEM, $^*P < 0.01$).

expression as they mature before mineralization.[22] Therefore, decreasing of ALP activity in calcifying VSMC blocks differentiation of VSMCs into osteoblastic cells. Furthermore, ALP can promote calcification by hydrolysing pyrophosphate. Thus, inhibition of ALP activity by NO may suppress calcification by a number of mechanisms. These findings suggest that NO regulates vascular calcification through inhibiting mineralization of VSMCs and differentiation of VSMCs into osteoblastic cells. On the other hand, the expression of NOS was induced in calcifying VSMCs. Our hypothesis is that